UNIVERSIDADE FEDERAL DO RIO GRANDE – FURG
INSTITUTO DE OCEANOGRAFIA
PROGRAMA DE PÓS-GRADUAÇÃO EM OCEANOGRAFIA BIOLÓGICA

GRUPOS FUNCIONAIS DE FITOPLÂNCTON A PARTIR DA REFLECTÂNCIA DE SUPERFÍCIE EM ÁGUAS COSTEIRAS

NIKOLAS URRUTIA HEINZ

Dissertação apresentada ao Programa de Pós-graduação em Oceanografia Biológica da Universidade Federal do Rio Grande - FURG, como requisito parcial à obtenção do título de MESTRE.

Orientadora: Profa. Dra. Maria Fernanda Coló Giannini

RIO GRANDE/RS, Brasil
Maio de 2026

GRUPOS FUNCIONAIS DE FITOPLÂNCTON A PARTIR DA REFLECTÂNCIA DE SUPERFÍCIE EM ÁGUAS COSTEIRAS

NIKOLAS URRUTIA HEINZ

Dissertação apresentada ao Programa de Pós-graduação em Oceanografia Biológica da Universidade Federal do Rio Grande - FURG, como requisito parcial à obtenção do título de MESTRE.

RIO GRANDE/RS, Brasil
Maio de 2026

© A cópia parcial e a citação de trechos desta dissertação/tese são permitidas sob a condição de que qualquer pessoa que a consulte reconheça os direitos autorais do autor. Nenhuma informação derivada direta ou indiretamente desta obra deve ser publicada sem o consentimento prévio e por escrito do autor.

H472g

Heinz, Nikolas Urrutia
Grupos funcionais de fitoplâncton a partir da reflectância de superfície em águas costeiras / Nikolas Urrutia Heinz. - 2026.
78f.

Dissertação (Mestrado) – Universidade Federal do Rio Grande – Programa de Pós-Graduação em Oceanografia Biológica, 2026.

Orientadora: Dra. Maria Fernanda Coló Giannini

1. Oceanografia Biológica. 2. Sensoriamento remoto. 3. Cor do oceano. 4. Águas de caso 2. 5. HPLC/CHEMTAX. 6. OCI/PACE. I. Giannini, Maria Fernanda Coló. II.Título.

CDU 573(26)

Catalogação na fonte: Bibliotecária Brenda Sequeira CRB10/1979

UNIVERSIDADE FEDERAL DO RIO GRANDE - FURG
IO – INSTITUTO DE OCEANOGRAFIA
PROGRAMA DE PÓS-GRADUAÇÃO EM OCEANOGRAFIA BIOLÓGICA
E-mail: ccpgob@furg.br – home-page: www.ppgocbio.furg.br

ATA DE DEFESA DE DISSERTAÇÃO DE MESTRADO – 02/2026

Às quatorze horas do dia quinze de maio do ano de dois mil e vinte e seis, de forma virtual sala: https://conferenciaweb.rnp.br/sala/maria-fernanda-colo-giannini-maria, Presencial: Auditório "João Rocha" IO - FURG/C. Carreiros, reuniu-se a Comissão Examinadora de Dissertação de Mestrado do Acad. **Nikolas Urrutia Heinz**, composta pelos seguintes membros: Profa. Dra. Maria Fernanda Coló Giannini – Orientadora - (PPGOB-IO/FURG); Profa. Dra. Margareth Copertino (PPGOB-IO-FURG), Profa. Dra. Priscila Lange (INPO), Prof. Dr. Marcio Souza (UFPel). Título da Dissertação: "GRUPOS FUNCIONAIS DE FITOPLÂNCTON A PARTIR DA REFLECTÂNCIA DE SUPERFÍCIE EM ÁGUAS COSTEIRAS". Dando início à reunião, a Coordenadora do PPGO, Profa. Dra. Silvina Botta, agradeceu a presença de todos e fez a apresentação da Comissão Examinadora. Logo após, explicou que o candidato teria um tempo de 45 a 60 min. para explanação do tema, e cada membro da Comissão, um máximo de 30 min. para perguntas. Dando prosseguimento, passou a palavra ao candidato que apresentou o tema e respondeu às perguntas formuladas. Após explanação, a Comissão aprovou o que segue: As sugestões de todos os membros da Comissão Examinadora, que seguem em pareceres em anexo, foram aceitas pela orientadora/candidato para incorporação na versão final. Foi atribuída a seguinte classificação ao candidato: Profa. Dra. Margareth Copertino - Classificação: Aprovado, Profa. Dra. Priscila Lange – Classificação: Aprovado e Prof. Dr. Marcio Souza - Classificação: Aprovado. O candidato foi considerado APROVADO por UNANIMIDADE. Nada mais havendo a tratar eu, Clabisnei Moura de Melo – Secretário do PPGOB lavra a presente ata que após lida e aprovada, será assinada pela Comissão Examinadora, pelo aluno e pela Coordenadora do PPGOB.

gov.br Documento assinado digitalmente
MARIA FERNANDA COLO GIANNINI
Data: 25/05/2026 22:27:40-0300
Verifique em https://validar.iti.gov.br

Profa. Dra. Maria Fernanda Coló Giannini
Orientadora

gov.br Documento assinado digitalmente
MARGARETH DA SILVA COPERTINO
Data: 20/05/2026 00:45:19-0300
Verifique em https://validar.iti.gov.br

Profa. Dra. Margareth Copertino

gov.br Documento assinado digitalmente
PRISCILA KIENTECA LANGE
Data: 19/05/2026 11:33:52-0300
Verifique em https://validar.iti.gov.br

Profa. Dra. Priscila Lange

gov.br Documento assinado digitalmente
MARCIO SILVA DE SOUZA
Data: 19/05/2026 15:38:03-0300
Verifique em https://validar.iti.gov.br

Prof. Dr. Marcio Souza

gov.br Documento assinado digitalmente
NIKOLAS URRUTIA HEINZ
Data: 20/05/2026 08:04:21-0300
Verifique em https://validar.iti.gov.br

Acad. Nikolas Urrutia Heinz

Profa. Dra. Silvina Botta
Coordenador a PPGOB

gov.br Documento assinado digitalmente
SILVINA BOTTA
Data: 25/05/2026 13:27:17-0300
Verifique em https://validar.iti.gov.br

AGRADECIMENTOS

Em primeiro lugar, agradeço aos meus pais, Michele e Philip, meu porto seguro e minha maior inspiração. Vocês me ensinaram tudo na vida e me incentivaram desde o começo, desde meus primeiros experimentos ainda criança, com água, erva-mate e detergente, até meu estranho sonho de trabalhar com imagens de satélite. Agradeço por todo o apoio, carinho e compreensão que vocês têm por mim, inclusive pelos puxões de orelha sempre que necessários (e digamos que isso acontece com mais frequência do que deveria). Agradeço por me ensinarem a sonhar alto e a querer desbravar o mundo. Sem vocês, eu não seria quem sou hoje e este trabalho é tão meu quanto de vocês.

Queria agradecer à minha família, aos meus avós, tios, tias, primos e primas. Obrigado pelo apoio, carinho e incentivo que vocês me deram ao longo dessa jornada pessoal e acadêmica. Agradeço por sempre estarem do meu lado, por sempre quererem o melhor para mim e por lutarem por isso. Agradeço por cada encontro, por cada palavra de apoio, por cada abraço, por toda a preocupação que vocês têm comigo. Eu realmente amo todos vocês! Gostaria de agradecer aos meus amigos, Hellen, Carol, Gina e Hugo, por cada momento de companheirismo e descontração, por cada sofrimento compartilhado e por cada loucura que passamos juntos. Vocês não largaram a minha mão e me ajudaram a chegar até aqui. Por isso, sou grato!

Agradeço à equipe do Labfito, pois cada um de vocês contribuiu para me ajudar nessa jornada. Agradeço ao Pedro, à Savênia e à Faby pelas conversas, pelos ensinamentos e pela paciência que vocês tiveram comigo. À Catharina, pela parceria, por todas as conversas e cafezinhos, tentando não surtar com os nossos trabalhos, mas sempre ajudando um ao outro. À Ana, pelos debates sobre cinema, mas também por sempre me apoiar, por sempre me incentivar a melhorar o meu trabalho, por sempre ter paciência e estar disponível a ajudar. Ao Prof. Rafael, por todos os ensinamentos, pela disponibilidade, pelo auxílio em diversas etapas deste trabalho. Por fim, não poderia deixar de agradecer à minha orientadora, Prof. Fernanda, que me acompanhou em cada etapa desta pesquisa, que sempre acreditou que eu conseguiria os resultados que consegui. Obrigado por sempre semear as melhores ideias e por sempre trazer os questionamentos mais difíceis. Obrigado por ser mais do que uma orientadora, uma amiga!

ÍNDICE

LISTA DE TABELAS……. III
LISTA DE FIGURAS……. IV
LISTA DE EQUAÇÕES…….. V
LISTA DE ACRÔNIMOS……. VI
RESUMO…….. VIII
ABSTRACT…… IX
PREFÁCIO……... 1
CAPÍTULO 1: INTRODUÇÃO……. 2
1. DIVERSIDADE DO FITOPLÂNCTON MARINHO……... 2
2. BIO-ÓPTICA MARINHA NA DETECÇÃO DE PFTs…… 7
3. OBJETIVOS……... 13
REFERÊNCIAS BIBLIOGRÁFICAS……. 13
CAPÍTULO 2: ARTIGO CIENTÍFICO…….. 20
1. INTRODUCTION…….. 21
2. METHODS…….. 23
2.1 Study Area……. 23
2.2 Data Acquisition and Analyses…… 26
2.3 EOF-based model for PFT retrieval……... 30
2.4. Application of the EOF-PFT model to satellite data…… 32
3. RESULTS…… 34
3.1 Total chlorophyll and phytoplankton community composition……... 34
3.2 EOF-based analysis of the Rrs data…… 35
3.3 PFT model evaluation……... 37
3.4 PFT model implementation on satellite data (PACE)..... 40
4. DISCUSSION…….. 42
4.1 PFT modelling from hyperspectral Rrs in the SWAO coastal waters……. 42
4.2 PFT distribution in the SWAO coast and its ecological and biogeochemical impacts……. 48
4.3 Future prospects for PFT estimates on hyperspectral sensors……. 50
5. CONCLUSION……... 51
ACKNOWLEDGEMENTS……... 53
REFERENCES……. 53
CAPÍTULO 3: CONCLUSÕES…… 65

LISTA DE TABELAS

Table 1. General information about the cruises used in this study, including the name, sampling region, period and the number of oceanographic stations (n).....26

Table 2. Estimated intercepts and EOF-based regression coefficients for each phytoplankton functional type (PFT) model……..38

Table 3. Performance metrics for EOF-based models for Total Chlorophyll-a (TChla) and seven Phytoplankton Functional Types (PFTs), including Full-fit statistics and Cross-validation (cv) statistics……...40

LISTA DE FIGURAS

Figura 1. Exemplo de diversidade do fitoplâncton……...4

Figura 2. Esquema conceitual dos processos ópticos na atmosfera e na água que determinam a quantidade e a natureza espectral da luz recebida por um sensor……...8

Figura 3. Exemplos de diferentes composições dos componentes opticamente ativos da água e seu impacto na cor do oceano…… 9

Figura 4. Exemplo de variabilidade no espectro de porcentagem de reflectância de diferentes grupos de fitoplâncton…… 12

Figura 5. Map showing the study area. The white circles indicate the sampling stations in the SWAO (Southwest Atlantic Ocean)..... 24

Figura 6. Schematic framework of the EOF-based model for predicting seven PFTs on hyperspectral remote sensing reflectance…… 30

Figura 7. Phytoplankton functional types (PFTs) in the Southwest Atlantic Ocean (SWAO) coastal waters……35

Figura 8. Remote sensing reflectance (Rrs) dataset……... 36

Figura 9. Distribution of the spectral loadings for the Empirical-Orthogonal Functions (EOF) modes derived from *in situ* hyperspectral remote sensing reflectance (Rrs).....37

Figura 10. Regressions between TChla and PFT chlorophyll-a concentrations determined by HPLC-CHEMTAX and those predicted by the EOF-based hyperspectral model……... 39

Figura 11. Spatial distribution of Total Chlorophyll-a (TChla, A), Diatoms (B), *Prochlorococcus* (C), Cryptophytes (D), Haptophytes (E), *Synechococcus* (F), Dinoglagellates (G) and Prasinophytes (H).....41

LISTA DE EQUAÇÕES

Equation 1. Diffuse attenuation coefficient for downwelling irradiance……... 28
Equation 2. Remote sensing reflectance for in-water system…… 28
Equation 3. Water leaving radiance……29
Equation 4. Remote sensing reflectance for above-water system……..29
Equation 5. EOF modes derivation…… 31
Equation 6. Modelled chlorophyll-a concentration of each PFT……. 31
Equation 7. Median absolute error (MDAE).....32
Equation 8. Median percentage difference (MDPD).....32
Equation 9. Bias…… 32
Equation 10. Spectral Convolution…… 33

LISTA DE ACRÔNIMOS

AIC – Akaike information criterion

BC – Brazil Current

BCF – Brazilian Continental Shelf

BMC – Brazil Malvinas Conluence Zone

BRDF – Bidirectional reflectance distribution function

CDOM – Matéria Orgânica Dissolvida Colorida

Chla – Clorofila-*a*

CZCS – Coastal Zone Color Scanner

DV-Chla – Divinil-clorofila-a

E_d – Downwelling spectral irradiance

EOF – Funções Ortogonais Empíricas

GLM - Generalized linear model

HyperCP – HyperInSPACE Community Processor

HPLC – High-Performance Liquid Chromatography

IOCCG – International Ocean Colour Coordinating Group

K_d – diffuse attenuation coefficient for downwelling irradiance

K_u – diffuse attenuation coefficient for upwelling irradiance

L_i – Sky radiance upwelling radiance

L_t – Total above-water radiance

L_u – Upwelling radiance

L_w – Water-leaving radiance

MC – Malvinas Currnt

MDAE – Median absolute error

MDPD – Median percentage difference

NAP – Partículas Não-Algais

NIR – Near-Infrared radiation

OCI – Ocean Color Instrument

OLCI – Ocean and Land Color Instrument

PACE – Plankton, Aerosol, Cloud, Ocean Ecosystem

PFT – Grupos Funcionais de Fitoplâncton

R – Pearson coefficient of correlation

RMSE – Root mean square error

Rrs – Reflectância do Sensoriamento Remoto

RS – Sensoriamento Remoto

RSR – Relative Spectral Response

SeaWiFS – Sea- viewing Wide Field of View Sensor

SST – Sea Surface Temperature

SVD – Singular value decomposition

SWAO – Southwestern Atlantic Ocean

TChla – Total Chlorophyll-a

TSM – Material Particulado em Suspensão

RESUMO

Devido à sua complexidade, o fitoplâncton é frequentemente classificado em Grupos Funcionais de Fitoplâncton (PFTs), facilitando a compreensão de seu papel na regulação climática, nos ciclos biogeoquímicos e nas teias tróficas. Diversos métodos permitem determinar a composição fitoplanctônica, com destaque para o uso de dados ópticos da cor do oceano. Esta pesquisa teve como objetivo empregar a reflectância hiperespectral *in situ* para propor modelos capazes de discriminar PFTs em uma região costeira de águas opticamente complexas, visando suas aplicações em dados derivados de satélite. Para tanto, foram realizados cruzeiros científicos com coleta simultânea de amostras para análise de pigmentos fitoplanctônicos e de reflectância hiperespectral de superfície. Modelos de PFTs baseados em grupos quimiotaxonômicos foram desenvolvidos utilizando funções ortogonais empíricas (EOF) e modelos lineares generalizados (GLM). O desempenho dos modelos foi avaliado por validação cruzada, cujos resultados indicaram estimativas bem-sucedidas para clorofila-*a* total (TChla) e para cinco grupos funcionais (diatomáceas, criptófitas, dinoflagelados, haptófitas e prasinófitas). Já para as classes de cianobactérias (*Prochlorococcus* e *Synechococcus*), o desempenho foi moderado e insatisfatório, respectivamente. Em um primeiro exercício de aplicação dos modelos a uma imagem do sensor OCI/PACE, observaram-se padrões espaciais dos PFTs consistentes com um gradiente costa-oceano, com dominância de diatomáceas em regiões costeiras eutróficas e de cianobactérias em águas oceânicas oligotróficas. Esses resultados fornecem evidência inicial de que os modelos propostos podem ser aplicados com confiabilidade a produtos de sensoriamento remoto, embora uma validação extensiva com dados independentes ainda seja necessária. Em síntese, este estudo representa um avanço significativo na estimativa remota de tipos funcionais de fitoplâncton, ao mesmo tempo que identifica claramente os desafios a serem superados para futuras aplicações operacionais.

Palavras-Chave: Sensoriamento Remoto; Cor do Oceano; Águas de Caso 2; HPLC/CHEMTAX; OCI/PACE.

ABSTRACT

Due to its complexity, phytoplankton is frequently classified into Phytoplankton Functional Types (PFTs), facilitating the understanding of their role in climate regulation, biogeochemical cycles, and trophic webs. Several methods allow the determination of phytoplankton composition, with emphasis on the use of ocean color optical data. This research aimed to employ *in situ* hyperspectral reflectance to propose models capable of discriminating PFTs in a coastal region with optically complex waters, aiming at their application to satellite data. To this end, scientific cruises were conducted with simultaneous collection of samples for pigment analysis and surface hyperspectral reflectance. PFT models based on chemotaxonomic groups were developed using Empirical Orthogonal Functions (EOF) and Generalized Linear Models (GLM). Model performance was assessed through cross-validation, whose results indicated successful estimates for total chlorophyll-*a* (TChla) and for five functional groups (diatoms, cryptophytes, dinoflagellates, haptophytes, and prasinophytes). For the cyanobacteria classes (*Prochlorococcus* and *Synechococcus*), performance was moderate and unsatisfactory, respectively. In a first exercise applying the models to an image from the OCI/PACE sensor, spatial patterns of PFTs consistent with a coast-ocean gradient were observed, with dominance of diatoms in eutrophic coastal regions and cyanobacteria in oligotrophic oceanic waters. These results provide initial evidence that the proposed models can be reliably applied to remote sensing products, although extensive validation with independent data is still needed. In summary, this study represents a significant advance in the remote estimation of phytoplankton functional types, while clearly outlining the challenges to be overcome for more reliable operational applications.

Keywords: Remote Sensing; Ocean Color; Case-2 Waters; HPLC/CHEMTAX; OCI/PACE.

PREFÁCIO

O autor dessa dissertação tem uma forte ligação com o sensoriamento remoto, tendo essa área do conhecimento sido parte do seu processo de formação como técnico em geoprocessamento e oceanólogo. Desde os primeiros momentos na universidade, ao envolver-se em projetos relacionados a cianobactérias e ao fitoplâncton de forma geral, esses micro-organismos fotossintetizantes tornaram-se parte central de sua trajetória acadêmica. Nesse contexto, surgiram questionamentos sobre como integrar essas duas áreas do conhecimento, cuja convergência foi encontrada na bio-óptica marinha. Inicialmente voltado à análise da biomassa fitoplanctônica, o interesse evoluiu para a discriminação de grupos funcionais de fitoplâncton (PFTs) no espaço, tema que passou a constituir uma questão central desta pesquisa.

Nesse sentido, a presente dissertação foi desenvolvida com o objetivo de contribuir para os estudos de PFTs a partir de estimativas de concentração derivadas de técnicas de sensoriamento remoto da cor do oceano. Desde a década de 1990, diversos grupos de pesquisa têm investigado a possibilidade de estimar PFTs a partir de observações espaciais. Os primeiros estudos evidenciaram limitações tecnológicas, especialmente relacionadas à resolução espectral dos sensores disponíveis à época. Nas décadas de 2010 e 2020, com lançamentos de sensores multiespectrais com mais bandas (eg. OLCI/Sentinel-3) e sensores hiperespectrais (eg. OCI/PACE), novos estudos e abordagens surgiram para a estimativa de PFTs, ampliando as possibilidades de investigação, de forma a desbravar essa nova fronteira do conhecimento.

Mas o conhecimento não se constrói sozinho, ele se apoia nas descobertas dos que nos antecederam. A pesquisa é um exercício contínuo, marcado por acertos e falhas, com uma única constante: nada é estático, tudo está em permanente transformação. Sob essa óptica, essa dissertação está dividida em quatro capítulos: (1) o primeiro de caráter introdutório, apresentando aspectos relacionados ao fitoplâncton e a bio-óptica marinha; (2) o segundo, onde são traçados os objetivos dessa dissertação de mestrado; (3) o terceiro, onde é proposto um artigo científico intitulado “EOF‐based Hyperspectral Model to retrieve Phytoplankton Functional Types on Coastal Waters”; e (4) o último, onde são apresentadas as considerações finais deste trabalho.

CAPÍTULO 1: INTRODUÇÃO

1. DIVERSIDADE DO FITOPLÂNCTON MARINHO

O fitoplâncton, grupo extremamente diverso e complexo de micro-organismos fotossintetizantes aquáticos, desempenha um papel ecológico intrínseco aos ambientes, tanto do ponto de vista biológico quanto do ponto de vista geoquímico (Field *et al.*, 1998; Salmaso et al., 2015). Apesar de representar cerca de 2% da biomassa fotossintética da Terra, esse grupo é responsável por cerca de 50% da produção primária líquida global (Field et al., 1998), atuando como base da teia trófica dos ambientes aquáticos e sendo a principal fonte de matéria e energia desses ambientes (Falkowski, 1994; Rousseaux & Gregg, 2015; Henson et al., 2021).

Além disso, o fitoplâncton tem papel crucial na regulação do clima e nos ciclos biogeoquímicos, estando diretamente associado com a absorção, fixação e soterramento de carbono, com a produção global de oxigênio, e com o afundamento e a ciclagem de nutrientes (Winder & Sommer, 2012). Adicionalmente, diferentes tipos de fitoplâncton também influenciam a bioecologia local, afetando a dinâmica de zooplâncton, peixes e mamíferos, como sugerido por Cury et al. (2008) no ecossistema de Benguela, onde o predomínio de flagelados favorece o crescimento de sardinhas, enquanto o predomínio de diatomáceas beneficia a anchoveta.

Sabe-se que o grupo em questão está presente em dois dos três domínios da vida, *Bacteria* e *Eukarya* (Blankenship, 2002; Simon et al., 2009), representados por uma ampla variedade de linhagens evolutivas dos principais clados da árvore da vida, que adquiriram a fotossíntese através do processo de endossimbiose (Simon et al., 2009; Johnson & Martiny, 2015). De maneira geral, apesar de décadas de estudos focados na diversidade do fitoplâncton marinho, o conhecimento sobre sua real diversidade e riqueza de espécies permaneceu por muito tempo limitado (Simon et al., 2009; Guiry, 2012).

As primeiras iniciativas mais robustas, com base em dados taxonômicos e morfológicos clássicos, estimaram a existência de 3.444 a 4.375 espécies de fitoplâncton marinho (Sournia et al., 1991). No entanto, análises moleculares em escala global, como as

realizadas pela expedição Tara Oceans, revelaram que o número de espécies morfologicamente descritas pode ser apenas uma fração da diversidade real (Ibarbalz et al., 2019). Para as linhagens eucarióticas, como diatomáceas, dinoflagelados e haptófitas, a diversidade ribossômica detectada foi tipicamente de três a oito vezes superior ao número de morfoespécies descritas, indicando a existência de linhagens ainda não cultivadas ou descritas dentro da comunidade planctônica (de Vargas et al., 2015; Ibarbalz et al., 2019).

Em uma escala global, a distribuição, a diversidade e a composição das comunidades fitoplanctônicas é marcada por forte regionalização, com diferentes grupos taxonômicos ocupando nichos ambientais distintos (Flombaum et al., 2013; Dutkiewicz et al., 2020; Li et al., 2023). Essa heterogeneidade espacial reflete uma combinação de fatores ambientais e biológicos, incluindo a disponibilidade e a razão de nutrientes, a temperatura, a intensidade luminosa e a ação da pastagem seletiva, que atuam de forma integrada na estruturação das comunidades (Striebel et al., 2012; Lehtinen et al., 2017; Dutkiewicz et al., 2020). As diatomáceas, por exemplo, dominam altas latitudes, mares marginais e zonas de ressurgência costeira, onde concentrações mais elevadas de nitrato e silicato e processos de mistura mais intensos da coluna d'água favorecem seu crescimento e diversidade (Dutkiewicz et al., 2020; Li et al., 2023). Em contrapartida, as cianobactérias, dos gêneros *Prochlorococcus* e *Synechococcus*, dominam em regiões mais oligotróficas, especialmente nos giros tropicais e subtropicais, e têm suas menores concentrações em latitudes mais altas (Flombaum et al., 2013).

Nesse sentido, os organismos do fitoplâncton apresentam uma natureza bastante diversa, do ponto de vista taxonômico, morfológico e fisiológico. Isso implica em diferenças significativas de morfologias celulares, funções bioquímicas, requisitos elementares, estratégias tróficas e sua relação com ciclos biogeoquímicos (Pan et al., 2010; Dutkiewicz et al., 2020; Figura 01). Em uma perspectiva biogeoquímica, podem ser observadas diferentes contribuições, como por exemplo, cianobactérias diazotróficas afetam mais significativamente o ciclo do nitrogênio, fixando o conteúdo atmosférico desse elemento, enquanto diatomáceas irão impactar na ciclagem da sílica, elemento utilizado para a produção de suas frústulas (Henson *et al.,* 2021). Já em uma visão morfométrica, o fitoplâncton menor tende a afundar mais lentamente e permanece por

mais tempo na camada de mistura, participando dos processos biogeoquímicos, enquanto células maiores afundam mais rápido e podem chegar até mesmo ao fundo antes mesmo de serem decompostas, levando os nutrientes associados a elas para o fundo por décadas (IOCCG, 2014).



Figura 1. Exemplo de diversidade do fitoplâncton. A) Rhizaria (*Bigelowiella natans*); B) Prasinófita (*Tetraselmis chuii*); C) Prasinófita (*Nephroselmis pyriformis*); D) Euglenozoa (*Eutreptiella sp.*); E) Criptófita (*Rhodomonas salina*); F) Haptófita

(*Scyphosphaera apsteinii*); G) Dinoflagelado (*Akashiwo sanguinea*); H) Diatomácea (*Coscinodiscus radiatus*). Fonte: Simon et al., 2009.

A alta variabilidade taxonômica e morfo-funcional do fitoplâncton levou à classificação desses organismos em Grupos Funcionais de Fitoplâncton (Phytoplankton Functional Types - PFT) (Nair *et al.*, 2008). Nesse contexto, a organização de PFTs se trata de agrupamentos conceituais do reservatório autotrófico marinho, onde as espécies fitoplanctônicas são classificadas com base em traços funcionais (eg. características únicas e mensuráveis que permitem a categorização dos organismos em grupos). Exemplos disso são agrupamentos por aspectos morfológicos, classes de tamanho ou funções ecológica/bioquímica comuns, mesmo que não tenham alguma relação do ponto de vista filogenético (Nair et al, 2008; Salmaso et al., 2015; IOCCG, 2014). Um conhecimento mais profundo dos PFTs é uma forma pragmática e essencial para a compreensão dos ciclos biogeoquímicos nos oceanos, atuando também como um importante indicador do funcionamento dos ecossistemas e da exportação trófica de carbono (Le Quéré et al., 2005; Dutkiewicz et al., 2020), além de ser uma importante ferramenta para a modelagem climática e ecológica (Brotas et al., 2023).

Existem inúmeros métodos disponíveis para quantificação e determinação da composição de espécies fitoplanctônicas nos oceanos, cada uma delas apresentando benefícios e limitações (Chase et al., 2017). Sabe-se que, no entanto, houve uma grande evolução desde as primeiras abordagens realizadas em microscópios ópticos até a abordagem voltada ao sensoriamento remoto da cor do oceano (IOCCG, 2014). No entanto, a complementaridade entre as diferentes técnicas é fundamental para superar as limitações individuais de cada método e obter uma caracterização mais completa da comunidade fitoplanctônica (Nair et al., 2008; Lombard et al., 2019).

As metodologias mais clássicas se baseiam na microscopia óptica, que permite a descrição detalhada da diversidade fitoplanctônica por observação direta (Johnson & Martiny, 2015). Essa metodologia é especialmente importante e relevante pois permite a identificação de organismos até a nível de espécies, uma vez que hajam características morfológicas distinguíveis para isso (Karlson et al., 2010). No entanto, essa metodologia apresenta limitações, pois pode ser laboriosa quando se há um grande número de amostras, apresenta uma capacidade limitada de identificar organismos menores (eg. nano e picoplâncton), bem como a necessidade de especialistas treinados,

além de ser um tipo de análise espaço-temporalmente limitada a coletas (Lombard et al., 2019). A citometria de fluxo atua como uma técnica complementar à microscopia, permitindo a quantificação eficiente de células menores, como *Prochlorococcus*, *Synechococcus* e picoeucariotos, que frequentemente escapam à identificação por métodos morfológicos tradicionais (Johnson & Martiny, 2015).

Entre os principais avanços neste campo pode-se destacar o uso de Cromatografia Líquida de Alta Eficiência (HPLC) como ferramenta para detectar e determinar a abundância de pigmentos marcadores quimiotaxonômicos do fitoplâncton (Wright et al., 2005; Barlow et al., 2008; Johnson & Martiny, 2015). Essa metodologia permite estimar as concentrações relativas dos grupos de fitoplâncton se utilizando de razões de pigmentos marcadores para determinar as contribuições de cada grupo para a biomassa total (Mendes et al., 2007; Lee et al., 2022). Esta abordagem tem a vantagem de cobrir toda a assembleia fitoplanctônica em uma única análise, fornecendo uma avaliação quantitativa da composição da comunidade, contudo pigmentos marcadores não são necessariamente únicos a um determinado grupo, podendo haver também variabilidade na pigmentação acessória dentro de um mesmo táxon, além desta análise estar espaço-temporalmente limitada a coletas (Johnson & Martiny, 2015).

Técnicas moleculares emergiram como ferramentas complementares para o estudo da diversidade fitoplanctônica, permitindo acessar uma escala de detalhe inovadora (Johnson & Martiny, 2015). O sequenciamento de DNA de nova geração possibilita a caracterização massiva de comunidades por meio de genes marcadores, revelando uma diversidade muito superior àquela conhecida por métodos morfológicos tradicionais (de Vargas et al., 2015). Essas abordagens fornecem não apenas informações taxonômicas, mas também sobre a diversidade funcional e as interações bióticas, como a mixotrofia e o parasitismo (Karlusich et al., 2020). No entanto, apresentam desafios significativos, uma vez que os dados gerados são complexos e de difícil análise, há vieses inerentes à amplificação genômica e a interpretação quantitativa é limitada por variações no número de cópias dos genes alvo (Johnson & Martiny, 2015).

Outra possibilidade para se estudar os PFTs é a utilização de dados ópticos, incluindo medições de absorção de luz e de medidas da cor da água, i.e., da reflectância espectral (Chase *et al.*, 2017). Essa metodologia, aplicada ao sensoriamento remoto da cor do

oceano, vem se tornado uma abordagem crescente nas últimas décadas (Lombard et al., 2019).

2. BIO-ÓPTICA MARINHA NA DETECÇÃO DE PFTs

O Sensoriamento Remoto (SR) da cor do oceano vem se tornando uma ferramenta essencial para diversos segmentos das ciências naturais, auxiliando na identificação e no monitoramento de feições ou padrões encontrados em diferentes regiões da superfície da água a partir de sensores a bordo de satélites, aeronaves e drones (Bukata et al., 1995; Kirk, 2010; Ventura et al., 2017). Trata-se de uma forma passiva de sensoriamento remoto em que o Sol atua como fonte primária, emitindo radiação eletromagnética que se propaga pelo espaço sob a forma de fótons, exibindo comportamento dual onda-partícula, sendo essa energia coletada pelos detectores dos sensores (Kirk, 2010). A energia oriunda do Sol abrange um amplo espectro que se estende de aproximadamente 100 nm a 4 mm, com seu pico de emissão na faixa do visível (400–700 nm), à qual o olho humano é sensível e cujo espectro de cores varia do violeta ao vermelho (Duffie & Beckman, 2006).

Uma vez que os fótons entram nos limites do sistema terrestre, inicia-se uma sucessão de processos de interação. Um esquema conceitual pode ser observado na Figura 02. Inicialmente, os fótons interagem com compostos e partículas da atmosfera, como nuvens, gases e aerossóis, sendo submetidos a fenômenos de absorção, espalhamento e transmissão (Seidlitz et al., 2001; Jensen, 2009). A absorção e o espalhamento dependem da afinidade espectral do alvo, onde a absorção ocorre quando parte da energia dos fótons é transferida para o alvo incidente e transformada em outras formas de energia; e o espalhamento, por sua vez, pode assumir diferentes formas (Rayleigh, Mie ou não seletivo), conforme a relação entre o comprimento de onda da radiação e o tamanho das partículas presentes na atmosfera, redistribuindo a radiação eletromagnética em múltiplas direções (Bukata et al., 1995; Kirk, 2010). Esses processos resultam em uma atenuação espectral que varia conforme as características físico-química dos objetos e o comprimento de onda da radiação incidente, e, são a base dos estudos de bio-óptica marinha (Seidlitz et al., 2001; Kirk, 2010).

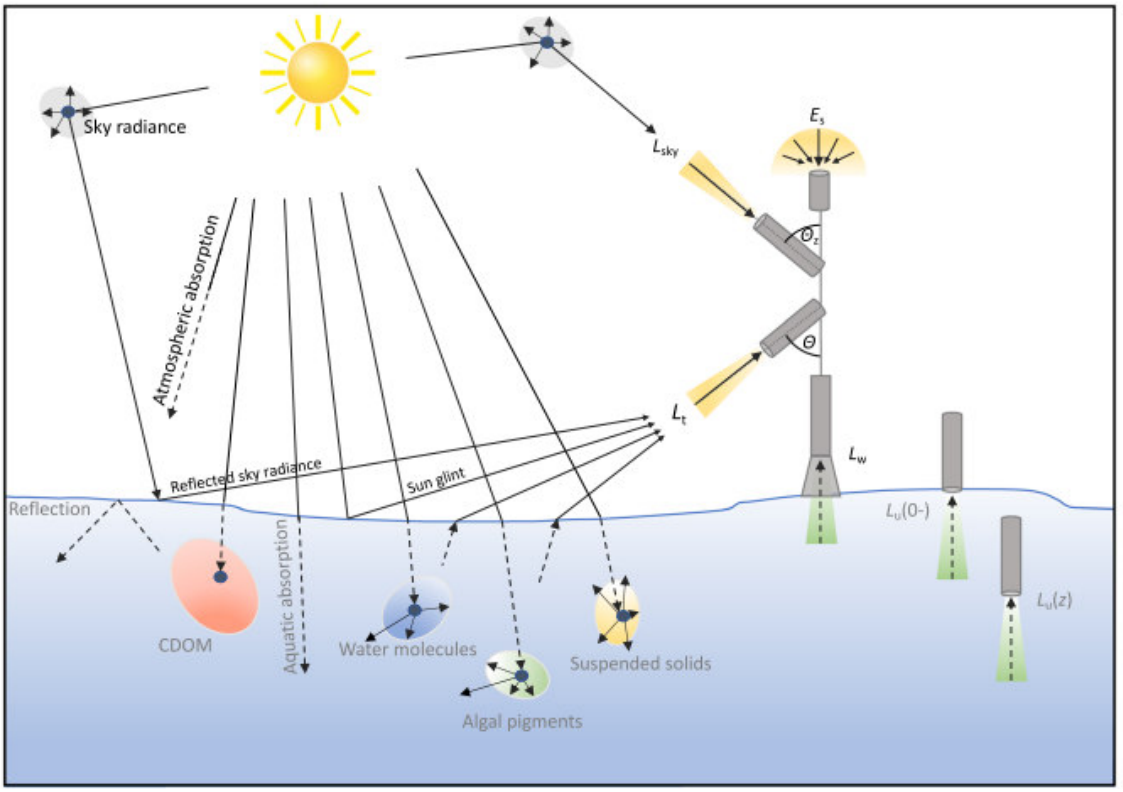


Figura 2. Esquema conceitual dos processos ópticos na atmosfera e na água que determinam a quantidade e a natureza espectral da luz recebida por um sensor. Fonte: Lehmann et al. (2023).

A parcela da radiação solar que é transmitida através da atmosfera pode então alcançar alvos na superfície terrestre, como oceanos e demais corpos d'água (Hoepffner & Zibordi, 2009; Morel, 2009; Kirk, 2010). Ao incidir sobre a superfície oceânica, parte da energia pode ser refletida especularmente ou quase especularmente (eg. sunglint), dependendo da rugosidade superficial, enquanto o restante penetra na coluna d'água (Bukata et al., 1995). Da fração que adentra o meio aquático, uma porção será absorvida e outra será espalhada pelos componentes opticamente ativos presentes na água. Em águas costeiras, esses componentes incluem o fitoplâncton, a matéria orgânica dissolvida colorida (Colored Dissolved Organic Matter - CDOM), o material em suspensão total (Total Suspended Matter - TSM) e partículas não algais (Non-Algal Particles - NAP), como detritos e formas coloidais, além da própria água pura, que também contribui para a atenuação da luz (Morel, 2009; Kirk, 2010).

Na coluna d'água, a radiação pode ser absorvida, sendo convertida em outras formas de energia, ou espalhada, tendo sua direção de propagação alterada. Esses processos

dependem do comprimento de onda e das características dos constituintes. Por exemplo, a clorofila-*a* (Chla) presente no fitoplâncton apresenta picos de absorção nos comprimentos de onda do azul e do vermelho (Morel, 2009), enquanto o TSM tem seu maior espalhamento nos comprimentos de onda do verde e do vermelho, o que por sua vez modifica a coloração da água (Doraxan et al., 2002). Um exemplo das diferentes colorações de água pode ser visto na Figura 03. A propagação dos fótons ocorre até que a energia luminosa seja exaurida na coluna d'água, em uma dada profundidade limite, ou até encontrar o fundo, em regiões mais rasas (Ackleson, 2003). Em regiões costeiras, a penetração da luz tende a profundidades menores, dada a maior complexidade óptica da água, influenciada por aportes terrígenos, descargas fluviais e maior concentração de partículas e matéria orgânica (Hoepffner & Zibordi, 2009).

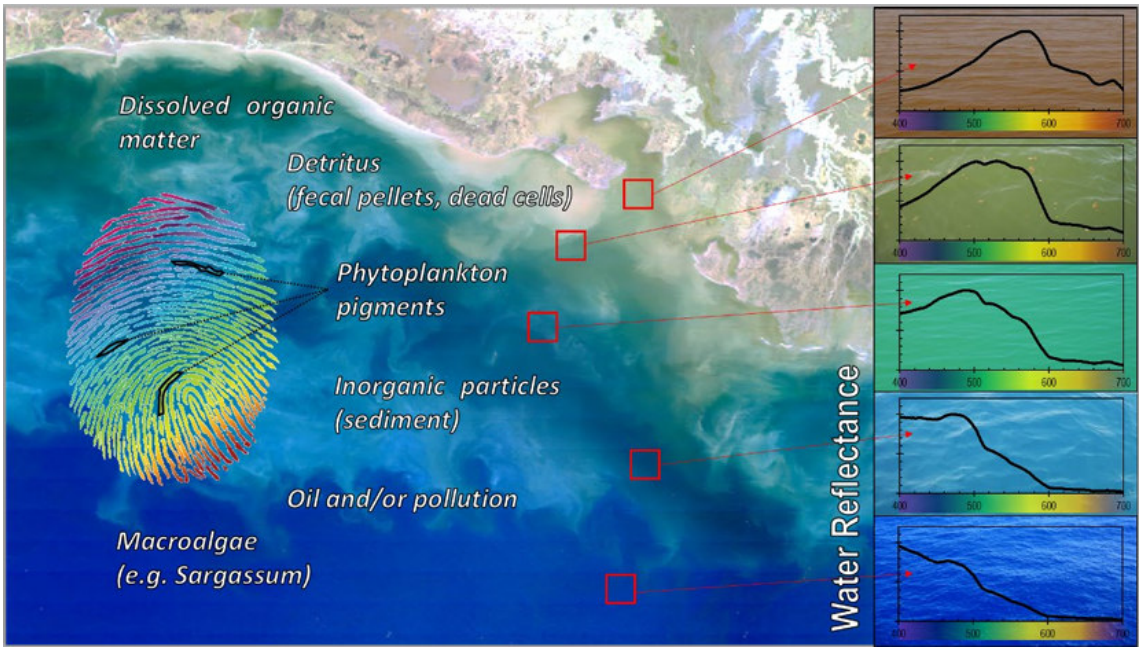


Figura 3. Exemplos de diferentes composições dos componentes opticamente ativos da água e seu impacto na cor do oceano. Fonte: Vandermeulen, 2025.

Parte da radiação que interage com a água e seus constituintes ópticos é direcionada de volta para a superfície, fenômeno denominado retroespalhamento, retornando à atmosfera carregando informações sobre a composição e a concentração dos componentes presentes (Morel, 2009). Esse sinal emergente sofre novamente atenuação ao atravessar a atmosfera até ser captado por sensores em diferentes plataformas. No caso dos satélites, a energia registrada pelo sensor percorre toda a espessura da atmosfera outra vez, sofrendo novamente processos de atenuação (Bukata et al, 1995;

Jensen, 2009). Contudo, o sinal registrado pelos sensores satelitais não corresponde exclusivamente à radiação refletida pela água, recebendo também contribuições da atmosfera e seus constituintes, do efeito de sunglint, e, em águas rasas, do efeito de fundo, incluindo sedimentos e organismos associados a ele (Doraxan et al., 2002; Hoepffner & Zibordi, 2009). Ressalta-se que, todavia, quando a medição é realizada em superfície, por radiômetros instalados em embarcações ou torres fixas, têm-se medidas de radiação refletida e de radiação incidente isentas das incertezas satelitais, especialmente no âmbito da correção atmosférica (Brando et al, 2016).

Nessa perspectiva, Bracher et al. (2020) apontam que dados radiométricos oriundos do sensoriamento remoto são a melhor forma de se monitorar os ecossistemas aquáticos, sendo uma importante ferramenta para avaliar a abundância e a biodiversidade do fitoplâncton. Isso porque o uso do sensoriamento remoto oferece uma maneira única de se obter dados com alta resolução espaço-temporal da superfície dos oceanos (Bracher et al. 2017), auxiliando na limitação que é observada em outras metodologias para estudos de grupos fitoplanctônicos (McClain, 2009). Outras estratégias observacionais, como cruzeiros e fundeios, não conseguem se aproximar da cobertura e resolução espaço-temporal dos sensores remotos, de forma que o uso dessas ferramentas pode ser fundamental para a obtenção de informações de PFTs, mesmo com resoluções ainda grosseiras e incertezas relativamente altas (IOCCG, 2014).

A história da estimativa do fitoplâncton por sensoriamento remoto remonta do final da década de 1960, quando experimentos embarcados em navios e aeronaves demonstraram pela primeira vez que a luz retroespalhada pelo oceano carregava informações sobre a concentração de Chla na superfície (Clarke et al., 1970). Os autores demonstraram que o aumento da Chla estava associado a uma diminuição relativa da radiação na região azul do espectro e a um acréscimo na região verde, estabelecendo a base para a oceanografia óptica por satélite. Esse princípio foi posteriormente incorporado ao Coastal Zone Color Scanner (CZCS), lançado em 1978, que produziu os primeiros mapas globais de Chla, e em satélites e missões subsequentes, como o Sea-viewing Wide Field of View Sensor (SeaWiFS) (Garver et al., 1994).

A Chla, é tida como o proxy mais utilizado da biomassa fitoplanctônica, uma vez que é uma forma pigmentar comum a todos os organismos presentes no fitoplâncton (Huot et

al., 2007). No entanto, a Chla por si só não fornece uma descrição completa da natureza complexa da estrutura e função da comunidade fitoplanctônica, uma vez não permite discriminar os diferentes grupos funcionais que compõem a comunidade (IOCCG, 2014; Bracher et al., 2017). Sabe-se, no entanto, que mesmo na atualidade a estimativa de PFTs por satélite é uma tarefa complexa (Nair et al., 2008; Bracher et al., 2017; Canuti, 2025). Ainda nos anos 90, Garver et al. (1994) apontaram que com as limitações tecnológicas e os sensores disponíveis na época, os quais eram multiespectrais, dificilmente seria possível desenvolver algoritmos robustos para a discriminação de grupos fitoplanctônicos.

Apesar disso, a importância ecológica e biogeoquímica dos PFTs estimulou o desenvolvimento de uma variedade de algoritmos para aplicação em SR da cor do oceano, seja para identificar grupos dominantes (Alvain et al., 2005, 2008; Mustapha et al., 2014; Navarro et al., 2014), obter classes de tamanho do fitoplâncton (Ciotti & Bricaud, 2006; Hirata et al., 2011; Brotas et al., 2013), derivar pigmentos acessórios (Pan et al., 2010; Bracher et al., 2015; El Hourany et al., 2019; Kramer et al., 2022), estimar a abundância celular (Thyssen et al., 2015; Lange et al., 2020) ou ainda derivar a concentração de clorofila de cada PFT (Moisan et al., 2017; Li et al., 2019; Xi et al., 2020; Vishnu et al., 2022).

Na atualidade, o uso de algoritmos baseados em Funções Ortogonais Empíricas (Empirical Orthogonal Function - EOF) vem se mostrando uma forma bastante acurada de se estimar a concentração de Chla de PFTs (Bracher et al., 2020), avaliando a variância ou forma espectral nos dados de reflectância da superfície ou da reflectância do sensoriamento remoto (Rrs). Apesar disso, os métodos de sensoriamento remoto requerem medições in situ para sua validação e aprimoramento (Brando et al., 2016; Chase et al., 2017). Dados de reflectância hiperespectral são essenciais, fornecendo informações relativas à composição da comunidade fitoplanctônica, através de diferenças na forma e na magnitude do espectro de reflectância (Xi et al., 2017; Kramer et al., 2022).

Estes dados, obtidos por radiômetros, são isentos de erros associados às incertezas satelitais, como a correção atmosférica, e apresentam maior resolução espectral do que a maioria dos sensores satélites da cor do oceano, o que favorece a confecção de modelos

e algoritmos, especialmente na era de plataformas de maior resolução espectral (Xi et al., 2017). Isso ocorre em razão da variabilidade na absorção e no espalhamento de luz nos diferentes PFTs ocorrer em pequenas faixas espectrais específicas a cada grupo (eg., Figura 04), diferentemente de outros compostos opticamente ativos. Assim, uma maior disponibilidade de bandas radiométricas implica em uma maior representatividade desses organismos na reflectância da água (Kramer et al., 2022). Dessa forma, os dados *in situ* são utilizados na criação, validação e ajuste de sensores e modelos com maior resolução espectral.

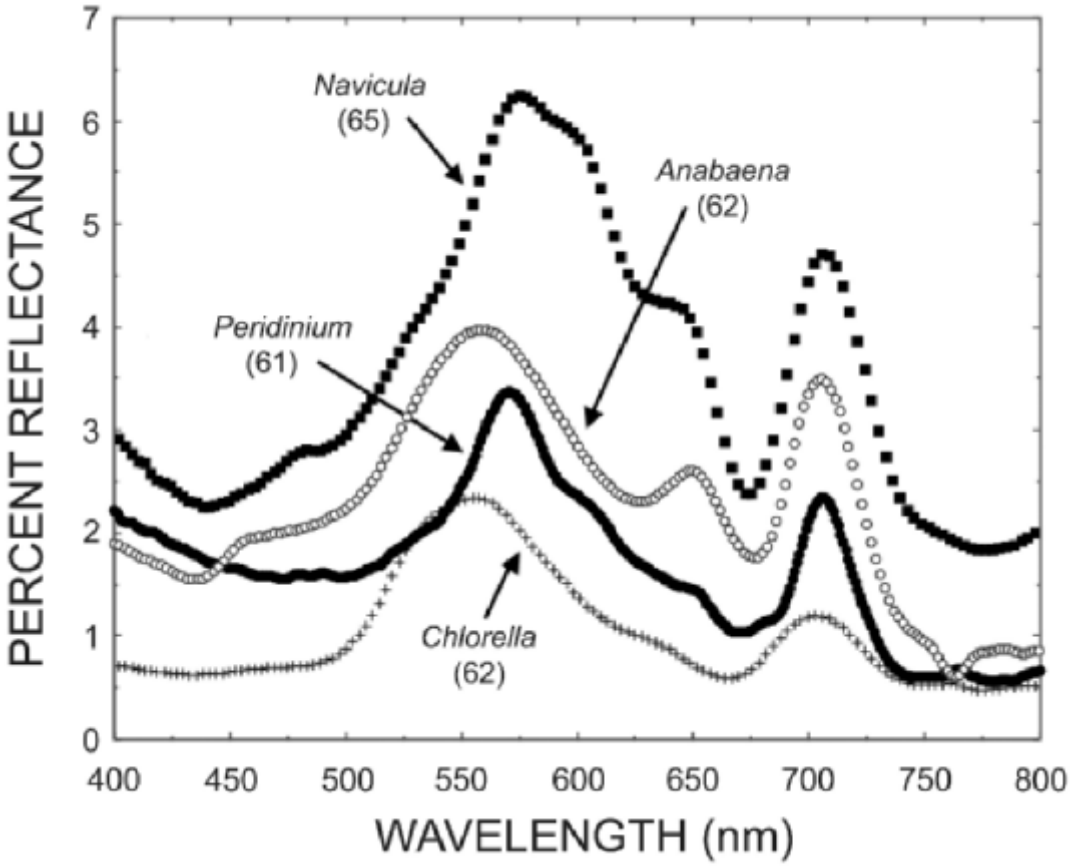


Figura 4. Exemplo de variabilidade no espectro de porcentagem de reflectância de diferentes grupos de fitoplâncton em cultivo. Fonte: Schalles, 2006.

Nesse sentido, o lançamento do sensor Ocean and Land Color Instrument (OLCI), a bordo do satélite Sentinel-3 da ESA, trouxe avanços nessa problemática de PFTs, com maior resolução espectral, ainda que permaneça no campo multiespectral (Brewin et al., 2017; Vishnu et al., 2022; McKibben et al., 2024). Todavia, o lançamento de missões satelitais hiperespectrais, como as missões Plankton, Aerosol, Cloud, Ocean Ecosystem (PACE), Environmental Mapping and Analysis Program (EnMAP) e Hyperspectral

Precursor of the Application Mission (PRISMA), fornecem uma perspectiva futura extremamente favorável para estudos voltados a composição da comunidade fitoplâncton global (Werdell et al., 2019; Lange et al., 2020; Cetinić et al., 2024). Portanto, essa pesquisa pretende propor modelos regionais de PFTs na superfície do mar a partir de dados *in situ* de reflectância hiperespectral, avaliando sua aplicabilidade em dados de sensoriamento remoto em águas costeiras.

3. OBJETIVOS

Objetivo Geral:

Propor modelos bio-ópticos para estimar a concentração de grupos funcionais de fitoplâncton (PFTs) a partir da reflectância hiperespectral de superfície, em regiões costeiras, visando a aplicação dos mesmos para detecção remota desses grupos.

Objetivos Específicos:

I. Quantificar e descrever os diferentes grupos fitoplanctônicos encontrados na costa sul-sudeste do Brasil em campanhas oceanográficas realizadas entre 2011 e 2025.
II. Identificar os modos dominantes de variabilidade da reflectância hiperespectral de superfície na área de estudo, relacionando-os a diferentes PFTs;
III. Propor e auto-validar modelos de estimativa de concentração dos PFTs baseados na reflectância hiperespectral *in situ*;
IV. Avaliar mapas de distribuição espacial dos PFTs estimados a partir dos modelos propostos em imagens do sensor hiperespectral OCI, a bordo da missão PACE (Plankton, Aerosol, Cloud, Ocean Ecosystem).

REFERÊNCIAS BIBLIOGRÁFICAS

Ackleson, S. G. (2003). Light in shallow waters: A brief research review. Limnology and Oceanography, 48(1, part 2), 323-328.

Alvain, S., Moulin, C., Dandonneau, Y., & Breon, F. M. (2005). Remote sensing of phytoplankton groups in case 1 waters from global SeaWiFS imagery. Deep Sea Research Part I: Oceanographic Research Papers, 52(11), 1989-2004.

Alvain, S., Moulin, C., Dandonneau, Y., & Loisel, H. (2008). Seasonal distribution and succession of dominant phytoplankton groups in the global ocean: A satellite view. Global Biogeochemical Cycles, 22(3).

Barlow, R., Kyewalyanga, M., Sessions, H., Van den Berg, M., & Morris, T. (2008). Phytoplankton pigments, functional types, and absorption properties in the Delagoa and Natal Bights of the Agulhas ecosystem. Estuarine, Coastal and Shelf Science, 80(2), 201-211.

Blankenship, R. E. (2002). Molecular mechanisms of photosynthesis. Blackwell Science.

Bracher, A., Taylor, M. H., Taylor, B., Dinter, T., Roettgers, R., & Steinmetz, F. (2015). Using empirical orthogonal functions derived from remote-sensing reflectance for the prediction of phytoplankton pigment concentrations. Ocean Science, 11(1), 139-158.

Bracher, A., Bouman, H. A., Brewin, R. J., Bricaud, A., Brotas, V., Ciotti, A. M., ... & Wolanin, A. (2017). Obtaining phytoplankton diversity from ocean color: a scientific roadmap for future development. Frontiers in Marine Science, 4, 55.

Bracher, A., Xi, H., Dinter, T., Mangin, A., Strass, V., Von Appen, W. J., & Wiegmann, S. (2020). High resolution water column phytoplankton composition across the Atlantic Ocean from ship-towed vertical undulating radiometry. Frontiers in Marine Science, 7, 235.

Brando, V. E., Lovell, J. L., King, E. A., Boadle, D., Scott, R., & Schroeder, T. (2016). The potential of autonomous ship-borne hyperspectral radiometers for the validation of ocean color radiometry data. Remote Sensing, 8(2), 150.

Brewin, R. J., Ciavatta, S., Sathyendranath, S., Jackson, T., Tilstone, G., Curran, K., et al. & Raitsos, D. E. (2017). Uncertainty in ocean-color estimates of chlorophyll for phytoplankton groups. Frontiers in Marine Science, 4, 104.

Brotas, V., Brewin, R. J., Sá, C., Brito, A. C., Silva, A., Mendes, C. R., ... & Sathyendranath, S. (2013). Deriving phytoplankton size classes from satellite data: Validation along a trophic gradient in the eastern Atlantic Ocean. Remote Sensing of Environment, 134, 66-77.

Brotas, V., Ferreira, A., Veloso, V., Tracana, A., Guerreiro, C. V., Tarran, G. A., ... & Groom, S. B. (2023). Assessing phytoplankton community composition in the Atlantic Ocean from in situ and satellite observations. Frontiers in Marine Science, 10, 1229692.

Bukata, R. P., Jerome, J. H., Kondratyev, A. S., & Pozdnyakov, D. V. (1995). Optical properties and remote sensing of inland and coastal waters. CRC Press.

Canuti, E. (2025). Phytoplankton functional types in the Black Sea. A regionalized algorithm for improving ecosystem monitoring by integrating In-Situ HPLC pigment analysis and satellite observations. Marine Pollution Bulletin, 220, 118360.

Cetinić, I., Rousseaux, C. S., Carroll, I. T., Chase, A. P., Kramer, S. J., Werdell, P. J., ... & Sayers, M. (2024). Phytoplankton composition from sPACE: Requirements, opportunities, and challenges. Remote Sensing of Environment, 302, 113964.

Chase, A. P., Boss, E., Cetinić, I., & Slade, W. (2017). Estimation of phytoplankton accessory pigments from hyperspectral reflectance spectra: toward a global algorithm. Journal of Geophysical Research: Oceans, 122(12), 9725-9743.

Ciotti, A. M., & Bricaud, A. (2006). Retrievals of a size parameter for phytoplankton and spectral light absorption by colored detrital matter from water‐leaving radiances at SeaWiFS channels in a continental shelf region off Brazil. Limnology and Oceanography: Methods, 4(7), 237-253.

Clarke, G. L., Ewing, G. C., & Lorenzen, C. J. (1970). Spectra of backscattered light from the sea obtained from aircraft as a measure of chlorophyll concentration. Science, 167(3921), 1119-1121.

Colwell, R. N. (1968). Remote sensing of natural resources. Scientific American, 218(1), 54-71.

Cury, P. M., Shin, Y. J., Planque, B., Durant, J. M., Fromentin, J. M., Kramer-Schadt, S., ... & Grimm, V. (2008). Ecosystem oceanography for global change in fisheries. Trends in Ecology & Evolution, 23(6), 338-346.

De Vargas, C., Audic, S., Henry, N., Decelle, J., Mahé, F., Logares, R., ... & Velayoudon, D. (2015). Eukaryotic plankton diversity in the sunlit ocean. Science, 348(6237), 1261605.

Doxaran, D., Froidefond, J. M., Lavender, S., & Castaing, P. (2002). Spectral signature of highly turbid waters: Application with SPOT data to quantify suspended particulate matter concentrations. Remote sensing of Environment, 81(1), 149-161.

Duffie, J. A., & Beckman, W. A. (2006). Solar engineering of thermal processes (3rd ed.). John Wiley & Sons.

Dutkiewicz, S., Cermeno, P., Jahn, O., Follows, M. J., Hickman, A. E., Taniguchi, D. A., & Ward, B. A. (2020). Dimensions of marine phytoplankton diversity. Biogeosciences, 17(3), 609-634.

El Hourany, R., Abboud‐abi Saab, M., Faour, G., Aumont, O., Crépon, M., & Thiria, S. (2019). Estimation of secondary phytoplankton pigments from satellite observations using self‐organizing maps (SOMs). Journal of Geophysical Research: Oceans, 124(2), 1357-1378.

Falkowski, P. G. (1994). The role of phytoplankton photosynthesis in global biogeochemical cycles. Photosynthesis research, 39: 235-258.

Field, C. B.; Behrenfeld, M. J.; Randerson, J. T.; & Falkowski, P. (1998). Primary production of the biosphere: integrating terrestrial and oceanic components. Science, 281(5374): 237-240.

Flombaum, P., Gallegos, J. L., Gordillo, R. A., Rincón, J., Zabala, L. L., Jiao, N., ... & Martiny, A. C. (2013). Present and future global distributions of the marine Cyanobacteria Prochlorococcus and Synechococcus. Proceedings of the National Academy of Sciences, 110(24), 9824-9829.

Garver, S. A., Siegel, D. A., & B. Greg, M. (1994). Variability in near‐surface particulate absorption spectra: What can a satellite ocean color imager see?. Limnology and Oceanography, 39(6), 1349-1367.

Guiry, M. D. (2012). How many species of algae are there? Journal of phycology, 48(5), 1057-1063.

Henson, S. A., Cael, B. B., Allen, S. R., & Dutkiewicz, S. (2021). Future phytoplankton diversity in a changing climate. Nature communications, 12(1), 5372.

Hirata, T., Hardman-Mountford, N. J., Brewin, R. J. W., Aiken, J., Barlow, R., Suzuki, K., ... & Yamanaka, Y. (2011). Synoptic relationships between surface Chlorophyll-a and diagnostic pigments specific to phytoplankton functional types. Biogeosciences, 8(2), 311-327.

Hoepffner, N., & Zibordi, G. (2009). Remote sensing of coastal waters. In Steele, J. H.; Thorpe, S. A.; & Turekian, K. K (Eds.), Measurement techniques, platforms and sensors (pp. 492–501). Academic Press.

Huot, Y., Babin, M., Bruyant, F., Grob, C., Twardowski, M. S., & Claustre, H. (2007). Does chlorophyll a provide the best index of phytoplankton biomass for primary productivity studies?. Biogeosciences discussions, 4(2), 707-745.

Ibarbalz, F. M., Henry, N., Brandão, M. C., Martini, S., Busseni, G., Byrne, H., ... & Zinger, L. (2019). Global trends in marine plankton diversity across kingdoms of life. Cell, 179(5), 1084-1097.

IOCCG (2014). Phytoplankton Functional Types from Space. Sathyendranath, S. (ed.), Reports of the International Ocean-Colour Coordinating Group, No. 15, IOCCG, Dartmouth, Canada.

Jensen, J. R. (2009). Sensoriamento remoto do ambiente: Uma perspectiva em recursos terrestres (2ª ed.). Parêntese Editora.

Johnson, Z. I., & Martiny, A. C. (2015). Techniques for quantifying phytoplankton biodiversity. Annual Review of Marine Science, 7(1), 299-324.

Karlson, B., Godhe, A., Cusack, C., & Bresnan, E. (2010). Introduction to methods for quantitative phytoplankton analysis. In Karlson, B., Cusack, C., & Bresnan, E. (Eds.), Microscopic and molecular methods for quantitative phytoplankton analysis (pp. 1–9). UNESCO.

Karlusich, J. J. P., Ibarbalz, F. M., & Bowler, C. (2020). Phytoplankton in the Tara ocean. Annual Review of Marine Science, 12(1), 233-265.

Kirk, J. T. O. (2010). Light and photosynthesis in aquatic ecosystems (3rd ed.). Cambridge University Press.

Kramer, S. J., Siegel, D. A., Maritorena, S., & Catlett, D. (2022). Modeling surface ocean phytoplankton pigments from hyperspectral remote sensing reflectance on global scales. Remote Sensing of Environment, 270, 112879.

Lange, P. K., Werdell, P. J., Erickson, Z. K., Dall'Olmo, G., Brewin, R. J., Zubkov, M. V., ... & Cetinić, I. (2020). Radiometric approach for the detection of picophytoplankton assemblages across oceanic fronts. Optics Express, 28(18), 25682-25705.

Lee, M., Kim, Y. B., Park, C. H., & Baek, S. H. (2022). Characterization of seasonal phytoplankton pigments and functional types around offshore island in the East/Japan Sea, based on HPLC pigment analysis. Sustainability, 14(9), 5306.

Lehmann, M. K., Gurlin, D., Pahlevan, N., Alikas, K., Conroy, T., Anstee, J., ... & Yue, L. (2023). GLORIA-a globally representative hyperspectral in situ dataset for optical sensing of water quality. Sci. Data 10, 100.

Lehtinen, S., Tamminen, T., Ptacnik, R., & Andersen, T. (2017). Phytoplankton species richness, evenness, and production in relation to nutrient availability and imbalance. Limnology and Oceanography, 62(4), 1393-1408.

Li, Z., Sun, D., Wang, S., Huan, Y., Zhang, H., Liu, J., & He, Y. (2023). A global satellite observation of phytoplankton taxonomic groups over the past two decades. Global Change Biology, 29(16), 4511-4529.

Lombard, F., Boss, E., Waite, A. M., Vogt, M., Uitz, J., Stemmann, L., ... & Appeltans, W. (2019). Globally consistent quantitative observations of planktonic ecosystems. Frontiers in Marine Science, 6, 196.

McClain, C. R. (2009). A decade of satellite ocean color observations. Annual Review of Marine Science, 1(1), 19-42.

McKibben, S. M., Schollaert Uz, S., & Palacios, S. L. (2024). Testing a hyperspectral, bio‐optical approach to identification of phytoplankton community composition in the Chesapeake Bay estuary. Earth and Space Science, 11(5), e2023EA003244.

Mendes, C. R., Cartaxana, P., & Brotas, V. (2007). HPLC determination of phytoplankton and microphytobenthos pigments: comparing resolution and sensitivity of a C18 and a C8 method. Limnology and Oceanography: Methods, 5(10), 363-370. https://doi.org/10.4319/lom.2007.5.363.

Moisan, T. A., Rufty, K. M., Moisan, J. R., & Linkswiler, M. A. (2017). Satellite observations of phytoplankton functional type spatial distributions, phenology, diversity, and ecotones. Frontiers in Marine Science, 4, 189.

Morel, A. (2009). Bio-optical models. In Steele, J. H.; Thorpe, S. A.; & Turekian, K. K (Eds.), Measurement techniques, platforms and sensors (pp. 247–256). Academic Press.

Mustapha, Z. B., Alvain, S., Jamet, C., Loisel, H., & Dessailly, D. (2014). Automatic classification of water-leaving radiance anomalies from global SeaWiFS imagery: application to the detection of phytoplankton groups in open ocean waters. Remote sensing of environment, 146, 97-112.

Nair, A., Sathyendranath, S., Platt, T., Morales, J., Stuart, V., Forget, M. H., Devred, E., & Bouman, H. (2008). Remote sensing of phytoplankton functional types. Remote Sensing of Environment, 112(8), 3366-3375.

Navarro, G., Alvain, S., Vantrepotte, V., & Huertas, I. E. (2014). Identification of dominant phytoplankton functional types in the Mediterranean Sea based on a regionalized remote sensing approach. Remote Sensing of Environment, 152, 557-575.

Pan, X., Mannino, A., Russ, M. E., Hooker, S. B., & Harding Jr, L. W. (2010). Remote sensing of phytoplankton pigment distribution in the United States northeast coast. Remote Sensing of Environment, 114(11), 2403-2416.

Rousseaux, C. S., & Gregg, W. W. (2015). Recent decadal trends in global phytoplankton composition. Global Biogeochemical Cycles, 29(10), 1674-1688.

Salmaso, N., Naselli‐Flores, L., & Padisák, J. (2015). Functional classifications and their application in phytoplankton ecology. Freshwater biology, 60(4), 603-619.

Schalles, J. F. (2006). Optical remote sensing techniques to estimate phytoplankton chlorophyll a concentrations in coastal waters with varying suspended matter and CDOM concentrations. In L. L. Richardson & E. F. LeDrew (Eds.), Remote sensing of aquatic coastal ecosystem processes: Science and management applications (pp. 27–79). Springer.

Seidlitz, H. K., Thiel, S., Krins, A., & Mayer, H. (2001). Solar radiation at the Earth's surface. Comprehensive series in photosciences, 3, 705-738.

Simon, N., Cras, A. L., Foulon, E., & Lemée, R. (2009). Diversity and evolution of marine phytoplankton. Comptes rendus biologies, 332(2-3), 159-170.

Sournia, A., Chrdtiennot-Dinet, M. J., & Ricard, M. (1991). Marine phytoplankton: how many species in the world ocean?. Journal of Plankton Research, 13(5), 1093-1099.

Striebel, M., Singer, G., Stibor, H., & Andersen, T. (2012). “Trophic overyielding”: phytoplankton diversity promotes zooplankton productivity. Ecology, 93(12), 2719-2727.

Thyssen, M., Alvain, S., Lefebvre, A., Dessailly, D., Rijkeboer, M., Guiselin, N., ... & Artigas, L. F. (2015). High-resolution analysis of a North Sea phytoplankton community structure based on in situ flow cytometry observations and potential implication for remote sensing. Biogeosciences, 12(13), 4051-4066.

Ventura, D., & Bonifazi, A. (2017). Unmanned aerial systems (UASs) for environmental monitoring: A review with applications in coastal. In Mejia, O. D. L., & Escobar, J. (Eds.), Aerial robots: Aerodynamics, control and applications (pp. 165–184). IntechOpen.

Vishnu, P. S., Xi, H., Belluz, J. D. B., Hussain, M. S., Bracher, A., & Costa, M. (2022). Seasonal dynamics of major phytoplankton functional types in the coastal waters of the west coast of Canada derived from OLCI Sentinel 3A. Frontiers in Marine Science, 9, 1018510.

Werdell, P. J., Behrenfeld, M. J., Bontempi, P. S., Boss, E., Cairns, B., Davis, G. T., ... & Remer, L. A. (2019). The plankton, aerosol, cloud, ocean ecosystem mission: status, science, advances. Bulletin of the American Meteorological Society, 100(9), 1775-1794.

Winder, M.; & Sommer, U. (2012). Phytoplankton response to a changing climate. Hydrobiologia, 698: 5-16.

Wright, S. W., Jeffrey, S. W., & Mantoura, R. F. C. (2005). Phytoplankton pigments in oceanography: Guidelines to modern methods. UNESCO Publishing.

Xi, H., Hieronymi, M., Krasemann, H., & Röttgers, R. (2017). Phytoplankton group identification using simulated and in situ hyperspectral remote sensing reflectance. Frontiers in Marine Science, 4, 272.

Xi, H., Losa, S. N., Mangin, A., Soppa, M. A., Garnesson, P., Demaria, J., ... & Bracher, A. (2020). Global retrieval of phytoplankton functional types based on empirical orthogonal functions using CMEMS GlobColour merged products and further extension to OLCI data. Remote Sensing of Environment, 240, 111704.

CAPÍTULO 2: ARTIGO CIENTÍFICO

Retrieval of phytoplankton functional types from hyperspectral reflectance in Southwestern Atlantic coastal waters

Nikolas Heinz [a,*] , Catharina Santos Cardoso [a], Ana Paula Piazza Forgiarini [a], Carlos Rafael Borges Mendes [a,b], Áurea M. Ciotti [c], Fernanda Giannini [a]

[a] Universidade Federal do Rio Grande. Instituto de Oceanografia. Laboratório de Fitoplâncton e Microorganismos Marinhos. Rio Grande, RS, 96203-900, Brazil.

[b] MARE – Marine and Environmental Sciences Centre/ARNET – Aquatic Research Network, Faculdade de Ciências, Universidade de Lisboa, Campo Grande, 1749–016 Lisboa, Portugal.

[c] Centro de Biologia Marinha (CEBIMar), Universidade de São Paulo – USP, São Sebastião, SP, Brasil.

[*] corresponding author: Nikolas Heinz (nikolasheinz01@gmail.com)

Abstract

Due to its complexity, phytoplankton are often represented as Phytoplankton Functional Types (PFTs), to facilitate understanding of their role in climate regulation, biogeochemical cycles, and trophic webs. Several methods currently estimate phytoplankton composition using ocean color data. This study aimed to employ in situ hyperspectral reflectance to develop and evaluate models for discriminating PFTs in a coastal region with optically complex waters, with a focus on their application to hyperspectral satellite data. To this end, scientific cruises were conducted with concurrent collection of samples for HPLC pigment analysis and hyperspectral surface reflectance data. PFT models based on chemotaxonomic groups were developed using Empirical Orthogonal Functions (EOF) and Generalized Linear Models (GLM). Model performance was assessed through cross-validation,indicating successful estimates ($R > 0.7$) for total chlorophylla (TChla) and five functional groups (diatoms, cryptophytes, dinoflagellates, haptophytes, and prasinophytes). For cyanobacteria (*Prochlorococcus* and *Synechococcus*), performance was moderate ($R = 0.66$) and unsatisfactory ($R = 0.37$), respectively. In an initial application to an image from the OCI/PACE sensor, the models estimated spatial patterns of PFTs consistent with the expected coastocean gradient in phytoplankton composition observed in the area, with diatom dominance nearshore and cyanobacteria in oligotrophic waters. Although these results indicated the potential for applying the models to remote sensing products, extensive validation with independent data is still needed. In summary, this study advances in the remote estimation of phytoplankton

functional types in optically complex waters, while highlighting challenges for more reliable operational applications.

Keywords: Remote Sensing; Ocean Color; Case-2 Waters; HPLC/CHEMTAX; OCI/PACE.

1. INTRODUCTION

Phytoplankton comprise an extremely diverse and complex group of aquatic photosynthetic microorganisms, playing a fundamental ecological role from both biological and geochemical perspectives (Field et al., 1998; Salmaso et al., 2015). Although they represent only about 2% of Earth's photosynthetic biomass, this group is responsible for approximately 50% of global net primary production (Field et al., 1998), acting as the base of the trophic web in aquatic environments and as the main source of matter and energy in these ecosystems (Falkowski, 1994; Rousseaux & Gregg, 2015; Henson et al., 2021). Furthermore, phytoplankton play a crucial role in climate regulation and biogeochemical cycles, being directly associated with carbon uptake, fixation and burial, global oxygen production, and nutrient cycling (Winder & Sommer, 2012).

This group of organisms exhibit a highly diverse taxonomic, morphological and physiological nature, which implies significant differences in cell morphologies, biochemical functions, elemental requirements, trophic strategies, and in their relationships with biogeochemical cycles (Pan et al., 2010; Dutkiewicz et al., 2020). This high variability has led to the classification of these organisms into Phytoplankton Functional Types (PFTs) (Nair et al., 2008), which constitutes a conceptual grouping based on functional traits, even without necessarily having a phylogenetic relationship (Nair et al., 2008; Salmaso et al., 2015; IOCCG, 2014). A deeper knowledge of PFTs is fundamental for understanding ocean biogeochemical cycles, also serving as an important indicator of ecosystem functioning and trophic carbon export (Le Quéré et al., 2005; Dutkiewicz et al., 2020), in addition to constituting a valuable tool for climate and ecological modeling (Brotas et al., 2023).

Several methods are available for quantifying and determining the composition of phytoplankton species in the oceans, each with its own benefits and limitations (Chase

et al., 2017). Great progress has been made from the first approaches using optical microscopy to current ocean color remote sensing techniques (IOCCG, 2014). Among the main advances, the use of High-Performance Liquid Chromatography (HPLC) stands out as a tool to determine the abundance of pigments defined as chemical markers of PFTs. Another possibility is the use of optical data, including light absorption measurements (Ciotti et al., 2002) and water spectral reflectance (Chase et al., 2017).

From this perspective, Bracher et al. (2020) pointed out that radiometric data obtained by remote sensing constitute a unique and powerful tool to monitor aquatic ecosystems, being an important tool to assess phytoplankton abundance and biodiversity. Remote sensing offers a unique way to obtain high spatiotemporal resolution data of the ocean surface, overcoming limitations present in other methodologies for studies of phytoplankton groups (McClain, 2009). Chlorophyll-a (Chla), the photosynthetic pigment present in all phytoplankton organisms, is traditionally used as the most common proxy for its biomass, and it is a product routinely derived from remote sensing techniques (Morel & Berthon, 1989; Huot et al., 2007; Stoer & Fennel, 2024). However, Chl-a alone does not provide a complete description of the complex structure and function of the phytoplankton community, because it does not allow discrimination of the different functional groups that has essential roles in the ocean functioning (IOCCG, 2014; Bracher et al., 2017).

The ecological and biogeochemical importance of PFTs has stimulated the development of a variety of algorithms for application in ocean color remote sensing, aiming from the identification of dominant groups (Alvain et al., 2005, 2008; Mustapha et al., 2014; Navarro et al., 2014) to obtaining phytoplankton size classes (Ciotti & Bricaud, 2006; Hirata et al., 2011; Brotas et al., 2013), derivation of accessory pigments (Pan et al., 2010; Bracher et al., 2015; El Hourany et al., 2019; Kramer et al., 2022), cell concentration (Thyssen et al., 2015; Lange et al., 2020) or chlorophyll-*a* concentration per PFT (Moisan et al., 2017; Li et al., 2019; Xi et al., 2020; Vishnu et al., 2022; Konik et al., 2024). Currently, algorithms based on Empirical Orthogonal Functions (EOF) have proven to be reasonably accurate for estimating PFT Chla concentrations (Bracher

et al., 2015; Xi et al., 2020), by assessing the variance or spectral shape in surface reflectance or remote sensing reflectance (Rrs) data.

Despite these advances, remote sensing methods require *in situ* measurements for validation and improvement (Chase et al., 2017). Hyperspectral reflectance data are essential, as they provide information about phytoplankton community composition through differences in the shape and magnitude of the reflectance spectrum (Xi et al., 2017; Kramer et al., 2022). Besides to overcome the atmospheric correction signal, a large source of uncertainty in the satellite data, the *in situ* radiometry usually provides higher spectral resolution than most ocean color satellites (Xi et al., 2017), favoring the development of models and algorithms, especially in the era of higher spectral resolution sensors (Kramer et al., 2022; Zhang et al., 2026). In this sense, the launch of the Ocean and Land Colour Instrument (OLCI) on board ESA's Sentinel-3 satellite has brought advances to the study of PFTs, offering higher spectral resolution, although it remains in the multispectral domain (Brewin et al., 2017; Vishnu et al., 2022; McKibben et al., 2024).

However, the launch of hyperspectral satellite missions, such as NASA's Plankton, Aerosol, Cloud, ocean Ecosystem (PACE) mission, provides an extremely favorable future perspective for studies focused on global phytoplankton community composition (Werdell et al., 2019; Lange et al., 2020; Cetinić et al., 2024). Considering the importance of assessing the phytoplankton functional groups and their dynamics from remote data, and given the recent advances in hyperspectral sensors on board satellites and UAVs, the main goal of this study was to develop a bio-optical regional model, based on the *in situ* hyperspectral reflectance data and pigments-based phytoplankton composition, to distinguish PFTs at the sea surface of the Southwestern Atlantic coastal waters, which represents the first regional model for estimating PFTs in this area.

2. METHODS

2.1 Study Area

The study area comprises the Brazilian Continental Shelf (BCS), located in the Southwestern Atlantic Ocean (SWAO), extending approximately between 20°S and 35°S (Fig. 05). This region encompasses two distinct zones of the BCF: the southeastern

shelf, between 20°S and 28.5°S, and the southern shelf, between 28.5°S and 35°S. The southeastern portion is characterized by a significant variation in its width, being narrower in the Abrolhos-Campos region and progressively widening southward, reaching its maximum extent of approximately 200 km from the coastline to the shelf break (Rodrigues & Lorenzzetti, 2001). In contrast, the southern continental shelf exhibits a more uniform morphology, with a mean width of about 140 km throughout its entire extension (Soares & Möller Jr., 2001).

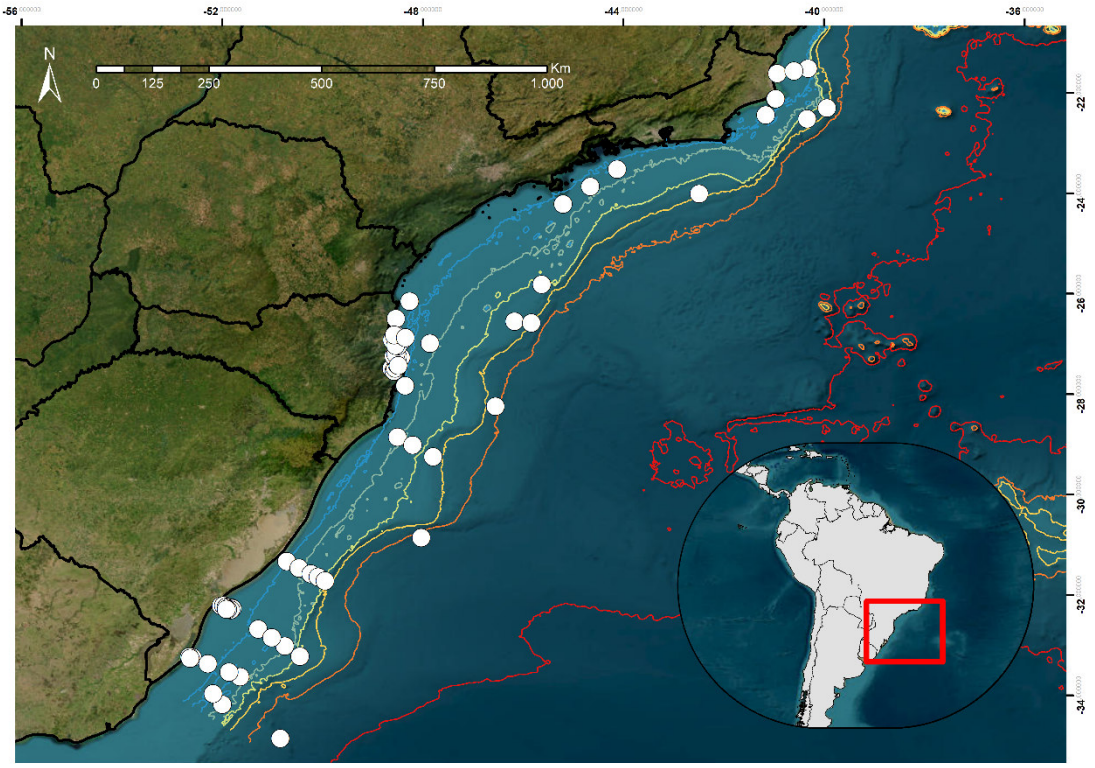


Figure 5. Map showing the study area. The white circles indicate the sampling stations in the SWAO (Southwest Atlantic Ocean). The colored lines mark the local depth isobaths, such as light blue (50 m), grayish green (100 m), light green (200 m), yellow(1000 m), orange (2000 m), and red (4000 m).

Ocean circulation in the region is dominated by two boundary currents flowing in opposite directions. The Brazil Current (BC) flows southward, transporting warm, saline, and oligotrophic waters along the continental slope (Möller Jr. et al., 2008). In contrast, the Malvinas Current (MC) moves northward with cold, nutrient-rich waters, influencing the outer shelf of the southern portion of the area (Möller Jr. et al., 2008; Piola et al., 2008a). The encounter of these two currents occurs in the Brazil-Malvinas

Confluence Zone (BMC), between approximately 35°S and 40°S, generating intense thermohaline gradients, high mesoscale variability, and elevated biological productivity (Garcia & Garcia, 2008; Pezzi et al., 2009).

The region is also influenced by coastal upwelling, particularly during austral spring and summer (Guimaraens & Coutinho, 1996; Mazzini & Barth, 2013). In the southeastern zone, the most prominent upwelling centre is located in Cabo Frio, where persistent northeasterly winds combined with a sharp change in coastline orientation and the local topography favour the ascent of cold, nutrient-rich South Atlantic Central Water to the surface (Rodrigues & Lorenzzetti, 2001). In the south zone, near Cabo de Santa Marta, coastal upwelling events also occur under similar wind forcing, promoting localised increases in phytoplankton biomass (Campos et al., 2013; Mazzini & Barth, 2013). Additionally, other smaller upwelling zones have also been observed along the southeastern shelf, including off São Sebastião and Cabo de São Tomé (Rodrigues & Lorenzzetti, 2001). All these upwelling features enhance biological productivity and locally modify sea surface temperature and nutrient concentrations, contributing to the biogeochemical heterogeneity of the study region (Carvalho et al., 2022).

The region receives strong influence from continental discharges, with the main input related to the La Plata River plume, which discharges a high load of freshwater onto the shelf (Piola et al., 2008b). The reach of this plume has a seasonal characteristic, reaching latitudes of 28°S in autumn and winter due to the impulse promoted by southeastern winds, whereas in summer and spring its reach is restricted due to the predominance of northeastern winds (Piola et al., 2000; Möller Jr. et al., 2008). Another very important input is related to the estuarine system of Patos Lagoon, which contributes with freshwater and sediment discharges that locally influence the properties of the southern shelf (Ciotti et al., 1995; Soares & Möller Jr., 2001).

The BCS region harbors several large metropolitan areas, including Rio de Janeiro, Vitória and Florianópolis (Dominguez, 2009), including several main port cities, such as Santos, Itajai and Rio Grande (Marta-Almeida et al., 2020). These urban areas are potential sources of freshwater and terrestrial runoff, nutrients, suspended particulate matter, and even urban/industrial effluents (Gonçalves-Araujo et al., 2018), which could locally influence the dynamics of the optical properties of surface waters and,

consequently, the remotely sensed ocean colour signal (Franz et al., 2021). Therefore, this region is characterized by a complex oceanic dynamic that includes the interaction of boundary currents (Carvalho et al., 2022), continental discharges (Piola et al., 2000, 2008b), and upwelling processes (Rodrigues & Lorenzzetti, 2001), resulting in an optically complex environment (Giannini et al., 2013). The region is classified as Case-2 waters, where light attenuation is influenced not only by water and phytoplankton but also by inorganic particulate material and colored dissolved organic matter (Garcia et al., 2005; Giannini et al., 2013).

2.2 Data Acquisition and Analyses

This section outlines the methodology for data acquisition and processing of phytoplankton pigment/PFT concentrations and hyperspectral remote sensing reflectance data. A total of six scientific cruises were conducted in the BCS region between 20 and 35°S (Table 01), associated with the ReNOMO, INCT Mar COI, and MCT-II projects, comprising 71 oceanographic stations with simultaneous collection of water samples for pigment analysis and radiometric data. Most of these stations were carried out in the austral summer and spring, inherently reflecting the conditions of those seasons.

Table 1. General information about the cruises used in this study, including the name, sampling region, period and the number of oceanographic stations (n). BCS - Brazilian Continental Shelf.

Cruise	Sampling region	Sampling period	Season	n
ReNOMO I	Southern-BCS	18 - 20 Oct. 2023	Spring	12
ReNOMO II	Southern-BCS	07 - 08 Oct. 2024	Spring	8
ReNOMO III	Southern-BCS	18 - 20 Mar. 2025	Summer	9
INCT Mar COI I	Southern-BCS	06 - 09 Nov. 2023	Spring	4
INCT Mar COI II	Southern-BCS	29 May - 04 Jun. 2024	Autumn	2
MCT II	S-SE-BCS	6 Dec 2010 - 11 Jan 2011	Summer	36

2.2.1 Phytoplankton pigments and PFT concentrations

In each station, water samples were filtered in dim light through Whatman GF/F filters, with pore size 0.7 μm and 25 mm diameter, using vacuum pressure system, under low pressure (≤5 mmHg). After this the samples were immediately frozen (–80°C) for later HPLC analysis.

The procedure for this analysis was carried out using an HPLC, from Shimadzu, with a C8 column, following the method of Zapata et al. (2000), which was discussed and

optimized by Mendes et al. (2007), and aligned with the international protocols established in the global intercalibration exercises promoted by the JCR - Joint Research Centre/European Commission (Canuti et al., 2022). Commercial pure pigment standards from the DHI (Institute for Water and Environment, Denmark) were used to calibrate the HPLC system.

Total Chlorophyll-*a* (TChla) concentrations were determined by the sum of monovinyl-chlorophyll-*a* (Chla) and divinyl-chlorophyll-*a* (DVChla) concentrations. The absolute and relative biomass concentration of each phytoplankton taxonomic group was calculated using CHEMTAX v1.95 (Mackey et al., 1996), based on a ratio matrix of class-specific accessory pigments and TChla. Seven chemotaxonomic groups were identified in the region: Prasinophytes (green flagellates), Diatoms, Dinoflagellates, Haptophytes, Cryptophytes, *Synechococcus* and *Prochlorococcus*. The initial pigment ratio matrix, adapted from Lima et al. (2019), included 16 phytoplankton pigments, with TChla serving as total biomass for all groups. To optimize the initial pigment ratio matrix, 60 matrices were generated by multiplying each ratio by a random function, following the approach described by Wright et al. (2009). The six output matrices with the lowest root mean square error (RMSE) residuals were averaged to obtain the final optimized result.

2.2.2 In Situ Hyperspectral Reflectance

The radiometric measurements carried out in this research employed two sets of hyperspectral radiometers: an above-water HyperSAS (Hyperspectral Surface Acquisition System) and a free-fall profiling in-water system, the HyperPRO, both equipped with the HyperOCR sensors, from Seabird. Although each instrument followed a distinct sampling and processing methodology, both ultimately provided the same variable, the remote sensing reflectance (Rrs).

2.2.2.1 In-water: HyperPRO

The radiometric data from the cruises conducted under the MCT-II project (2010-2011) were acquired using a free-fall profiler HyperPRO. The system comprises two hyperspectral sensors (350–800 nm, ~3.3 nm resolution), including a downward-facing HyperOCR-R measuring upwelling radiance (L_u) and an upward-facing HyperOCR irradiance sensor measuring downwelling irradiance (E_d). The equipment was freely

deployed from the vessel, collecting continuous vertical profiles of E_d (z) and L_u(z) at each station. To derive Rrs, the diffuse attenuation coefficients for downwelling irradiance (K_d) and for upwelling radiance (K_u) was estimated using the traditional K-analysis method (Smith & Baker, 1984, 1986) as the negative slope of the natural logarithm of E_d over a depth interval (Eq. 1).

$$K_d = -\frac{d}{dz}\left[ln\left(E_d(z)\right)\right] \quad (01)$$

Where K_d is diffuse attenuation coefficient for downwelling irradiance; z is the depth interval (m); and E_d is downwelling irradiance.

The same procedure is applied for K_u, based on the L_u(z) measurement. K_d(K_u) is computed between the E_d(L_u) measurements nearest the surface and either the first optical depth or the depth of the upper mixed layer, whichever is shallower (Zibordi et al., 2004). After obtaining K_d and K_u, the E_d and L_u profiles were extrapolated to just beneath the sea surface ($z = 0^-$) and then propagated to above the surface ($z = 0^+$) using refraction and transmission coefficients (Lee et al., 2013; Ruddick et al., 2019). Finally, the Rrs is calculated as shown in Eq. 2.

$$Rrs = \frac{L_W}{E_d(0^+)}\ [sr^{-1}] \quad (02)$$

Where L_w is the emergent radiation immediately above the surface; and E_d (0^+) is the solar irradiance immediately above the surface. The final output consists of Rrs spectra as a function of radiation wavelength.

2.2.2.2 Above-water HyperSAS

The radiometric data from the cruises conducted under the ReNOMO and INCT Mar COI projects (2023, 2024, and 2025) were acquired using the HyperSAS system, which is equipped with radiance and irradiance sensors positioned above the sea surface. This hyperspectral system operates within a wavelength range of 350 to 800 nm, comprising 136 high-resolution spectral channels.

The HyperSAS system employed includes two HyperOCR-R radiance sensors. One of these sensors was oriented toward the ocean to measure the total above-water radiance (L_t), while the other was directed toward the sky to provide sky radiance (L_i), both

expressed in μW cm^{-2} nm^{-1} sr^{-1} (Verma et al., 2021). The system also incorporates a HyperOCR irradiance sensor to measure downwelling spectral irradiance (E_d), in μW cm^{-2} nm^{-1}. In addition, a *tilt* sensor is coupled to the system and used as a data quality filter, since excessive inclinations may lead to spurious measurements originating from the other sensors (Mueller et al., 2003).

Data acquisition was carried out under favorable environmental conditions to ensure that the recorded signal was predominantly derived from the water column (Fargion & Mueller, 2000). Furthermore, the adopted observation geometry consisted of orienting the radiance sensors at a zenith viewing angle of 40°, and azimuth angles between 90° and 135° relative to the solar plane, with measurements collected for a minimum duration of five minutes at each station (Ruddick et al., 2019). From the radiometer outputs, it is possible to compute the water-leaving radiance (Eq. 3).

$$L_W = L_T - \rho L_i \quad (03)$$

Where L_w denotes the radiance emerging from the water surface after interaction with optically active constituents within the water column; ρ represents an estimate of sea surface reflectance, expressed as a function of solar–sensor geometry and wind speed (Mobley, 1999; Zhang et al., 2017). Finally, Rrs, in sr-1, was calculated (Eq. 4).

$$Rrs = \frac{L_W}{E_d} [sr^{-1}] \quad (04)$$

Where Rrs is the remote sensing reflectance and E_d is the downwelling solar irradiance. The mentioned processing was performed with HyperCP software (HyperInSPACE Community Processor; digital repository: https://github.com/nasa/HyperCP). HyperCP enables the application of a series of data quality corrections, including sunglint correction (Zhang et al., 2017), correction of near-infrared (NIR) residuals (Ruddick et al., 2006), and correction for the bidirectional reflectance distribution function (BRDF) effect (Lee et al., 2010). The final output consists of Rrs spectra as a function of radiation wavelength.

2.3 EOF-based model for PFT retrieval

Given that the PFT estimation model relies on two hyperspectral Rrs datasets acquired by two distinct radiometers, the initial step is to render them compatible by interpolating both datasets at a 0.1 nm interval. The methodology for model construction and validation follows the approach proposed by Bracher et al. (2015) and Xi et al. (2020), although it was adapted to the specific characteristics of our dataset. It is worth noting that different sample sizes (n) were used for each PFT model, as the occurrence of these groups varied across sampling stations. Stations where the concentration of a given PFT was zero were excluded from the construction of the respective model, ensuring that only non-zero concentrations were considered. Figure 06 presents the stepwise framework of the methodology.

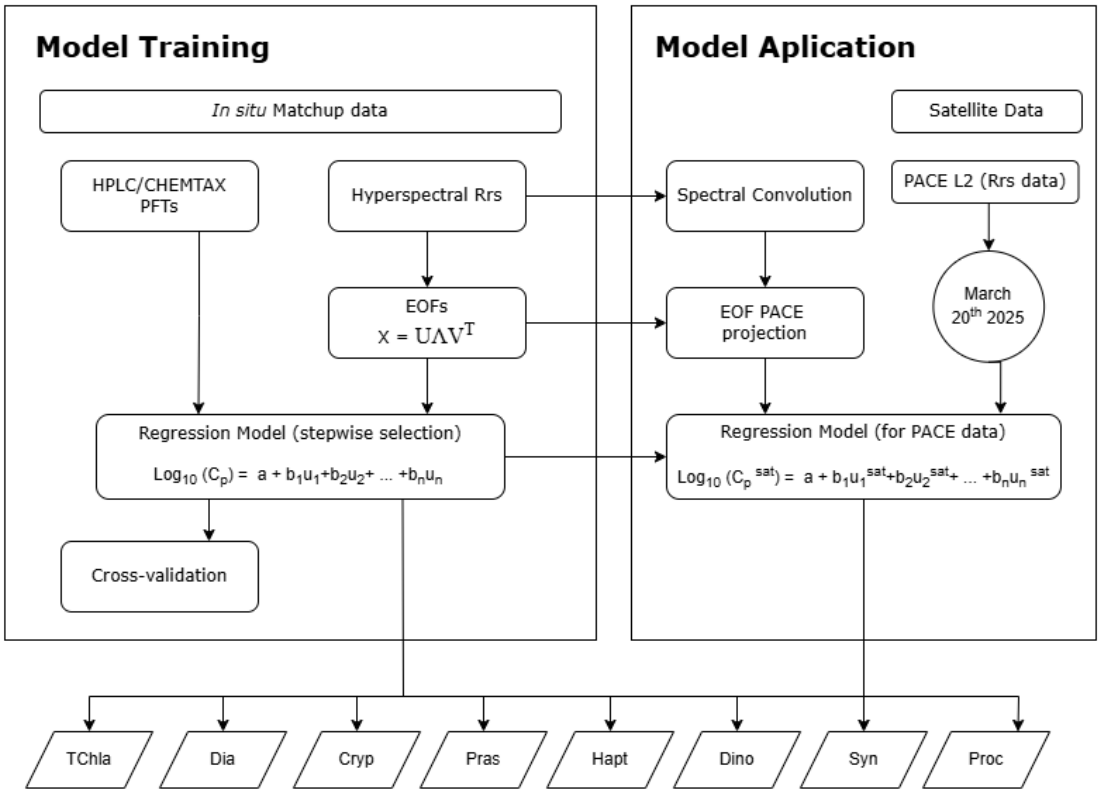


Figure 6. Schematic framework of the EOF-based model for predicting seven PFTs on hyperspectral remote sensing reflectance

Each Rrs spectrum was then standardized by subtracting the mean spectral value and subsequently dividing by the spectral standard deviation of the dataset (Taylor et al., 2013). The purpose of using EOF is to reduce the high dimensionality of the data and to

derive the dominant signals that best describe the variance within the dataset (Bracher et al., 2015). The standardized Rrs spectra were then subjected to a singular value decomposition (SVD) to derive the EOF modes, as shown in Eq. 5.

$$X = U\Lambda V^T \quad (5)$$

Where X is the standardized Rrs matrix; U is the matrix of scores (associated with EOF modes); Λ is singular values (general importance of each mode); V is the matrix of loadings (spectral pattern of each EOF); and the superscript T denotes the transposition of V matrix.

For the prediction of Chla for each PFT, generalized linear models (GLMs) were developed, expressing log-transformed Chla concentrations for each PFT (and for TChla as well) as a function of a subset of EOF scores. Only EOF modes whose standard deviations accounted for more than 1% of the standard deviation of the first EOF mode were selected as significant; the remaining modes were omitted (Xi et al., 2020). A stepwise automatic routine was used to select the most significant regression model by minimizing the Akaike information criterion (AIC). AIC estimates prediction error based on the number of scores, identifying the best model for the dataset (Bracher et al., 2015). The regression models for predicting each PFT are presented in Eq. 6.

$$log(C_P) = a + b_1u_1 + b_2u_2 + \ldots + b_nu_n \quad (6)$$

Where C_P is the Chla concentration of each PFT; a is the intercept; $b_{1, 2 \ldots n}$ are the regression coefficients; $u_{1, 2 \ldots n}$ are the EOF scores; and n is the number of EOF scores used by the model.

A repeated k-fold cross-validation technique was then applied. Specifically, a 10-fold cross-validation with 5 repetitions was used (Mnich et al., 2020). This method partitions the data into 10 subsets of approximately equal size; in each repetition, nine subsets are used for model training and the remaining subset for validation, with the process repeated 10 times so that each observation serves exactly once as validation data. The procedure is repeated five times to reduce the variability associated with the random partition (Yang et al., 2011). This approach is widely recognized to provide more stable

and less biased estimates of prediction error, particularly when the number of observations is limited (Kim, 2009; Mnich et al., 2020).

The regression model performance was also assessed by calculating the Pearson coefficient of correlation (R), median absolute error (MDAE, Eq. 7), median percentage difference (MDPD, Eq.8), and bias (Eq. 9) for the cross-validation (and for the whole dataset). R, MDAE, MDPD and bias were obtained using the $\log_{10}$-scaled predicted versus $\log_{10}$-scaled observed PFT Chla. The equations for these statistical metrics are given as follows:

$$MDAE = median_{i=1}^{M} \left| (C_{Pi} - C_{Oi}) \right| \quad (7)$$

$$MDPD = Median\ of \left[\frac{\left| (C_{Pi} - C_{Oi}) \right|}{C_{Oi}} \times 100 \right] \quad (8)$$

$$bias = \frac{100}{M} \sum_{i=1}^{M} \frac{(C_{Pi} - C_{Oi})}{C_{Oi}} \quad (9)$$

Where, M is the number of observations; C_O is observed PFT Chla.

2.4. Application of the EOF-PFT model to satellite data

The description of the data used and the steps employed in this example application of the PFT model to satellite data is presented in this section of the methodology. To this end, an Rrs product from the PACE mission was used, aiming to estimate the concentrations of the different PFTs and thus make a first evaluation of their suitability for this platform.

2.4.1 Plankton, Aerosol, Cloud, ocean Ecosystem (PACE) data

Rrs satellite data were obtained from the Ocean Color Instrument (OCI) onboard NASA's Plankton, Aerosol, Cloud, ocean Ecosystem (PACE) mission via the electronic repository of NASA's Earthdata (NASA, 2025a). OCI is a hyperspectral imaging radiometer that provides continuous spectral coverage from 340 to 890 nm with 5 nm bandwidth, with either 2.5 or 1.25 nm sampling, since March 2024 (Meister et al., 2024). The spatial resolution at nadir is approximately 1.2 km, with global coverage achieved within 1–2 days (Werdell et al., 2024). To avoid sun glint contamination over

ocean surfaces, OCI performs an along-track tilt maneuver of ±20° every orbit (Werdell et al., 2019). The instrument offers more than 120 visible spectral bands, a substantial increase compared to heritage multispectral sensors (Vandermeulen et al., 2025). Level 2 (L2) Rrs products were obtained from the ocean apparent optical properties suite and are currently available as provisional data (Werdell et al., 2024).

2.4.2 Spectral Convolution of *in situ* Rrs to PACE Rrs

In order to directly compare hyperspectral Rrs measurements obtained *in situ* with the Rrs products of OCI/PACE, a spectral convolution was applied, considering the relative Spectral Response (RSR) function of the sensors bands, which describes the detector's sensitivity at each wavelength within the bandwidth (Franke et al., 2006; Kumar & Mehta, 2024). The RSR is determined in the laboratory prior to launch and accounts for the optical characteristics of the system, including filters, mirrors, lenses, and the quantum efficiency of the detector (Meister et al., 2024). The RSR functions for OCI/PACE are available from the NASA Ocean Biology DAAC repository (https://oceancolor.gsfc.nasa.gov/resources/docs/rsr/sources/).

The spectral adjustment is applied to simulate what the sensor would measure while considering the differences between its spectral response and the field measurement. This is accomplished by numerically integrating over the entire wavelength range where the RSR is significantly greater than zero (Eq. 10). The result of the convolution is a single value per band, exactly what the satellite would measure if it were in place of the field instrument.

$$Rrs_{sim}(\lambda) = \frac{\int Rrs_{rad}(\lambda) \times RSR(\lambda) \times d\lambda}{\int RSR(\lambda) \times d\lambda} \quad (10)$$

Where, $Rrs_{sim}(\lambda)$ is the OCI/PACE simulated reflectance, $Rrs_{rad}(\lambda)$ is the reference hyperspectral data; and the RSR is the OCI/PACE Relative Spectral Response.

2.4.3 Applying EOF-based model on PACE data

The EOF-based PFT model was applied to an OCI/PACE image from March 20th 2025, to test the mapping of the spatial distribution of PFTs in a zone of SWAO. First, a new

EOF analysis was performed using the in situ Rrs data spectrally convolved to the PACE/OCI band set. This step yielded the EOF loadings and scores characterizing the spectral variability of the simulated data. Subsequently, to derive PFT Chl-a concentrations from the satellite imagery, the OCI/PACE Rrs data were standardized and projected onto the EOF loadings, generating a new set of EOF scores.

These new scores were then used in the regression equation (Eq. 6) to retrieve the spatial distribution of Chl-a for each PFT, employing the regression coefficients and intercepts previously determined from the EOF analysis of the in situ convolved data. Finally, spatial maps were produced for TChl-a and for the following PFTs: Prasinophytes (Pras), Diatoms (Dia), Dinoflagellates (Dino), Haptophytes (Hapt), Cryptophytes (Cryp), *Synechococcus* (Syn) and *Prochlorococcus* (Proc).

3. RESULTS

3.1 Total chlorophyll-*a* and phytoplankton community composition

Surface TChla varied considerably among the different oceanographic samplings in the SWAO, ranging from 0.05 to 13.71 mg m^{-3} (Figure 7). The highest concentrations were associated with periods of microalgal blooms off the coast of Santa Catarina/Brazil, in October 2023 and October 2024 (Figures 7a and 7b). Nevertheless, some stations within the lowest latitudinal band (20–25°S) deviated from this general pattern. Stations 80a and 80c close to Cape São Tomé, as well as stations 70 and 71 near the mouth of the Paraíba do Sul River, showed higher phytoplankton biomass and diversity than adjacent stations at similar latitudes (Figure 7f).

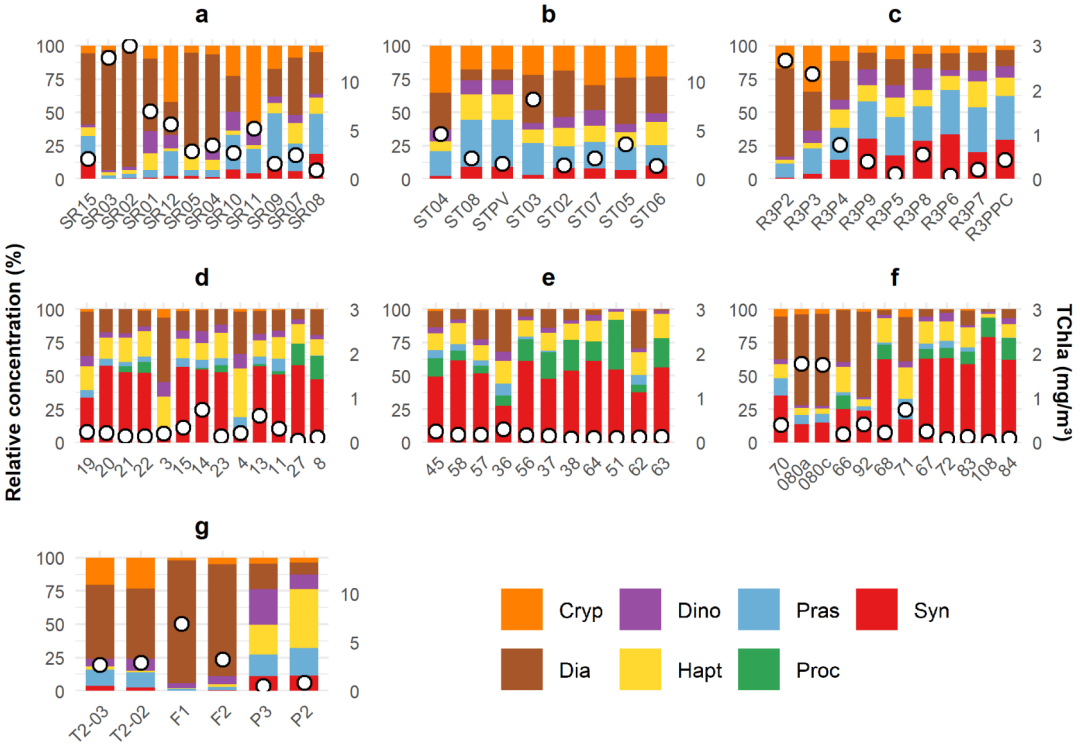


Figure 7. Phytoplankton functional types (PFTs) in the Southwest Atlantic Ocean (SWAO) coastal waters. The primary y-axis shows the relative contribution (%), and the secondary y-axis (white circles) shows the total phytoplankton biomass (in TChla [mg.m^{-3}]). Letters separated by cruises or projects, with columns arranged from left to right in order of increasing distance between the station and the coastline. a) ReNOMO I; b) ReNOMO II; c) ReNOMO III; d) MCT II: 30-35°S; e) MCT II: 25-30°S; f) MCT II: 20-25ºS; g) INCT Mar COI.

Similarly, Figure 7 also allows the observation of a clear differentiation in community structure along the coast-offshore axis. At stations closest to the coastline, characterized diatoms predominated overwhelmingly, followed by minor contributions from cryptophytes and dinoflagellates. Moving towards the outer shelf and slope, a gradual replacement of these dominant groups by picoplanktonic forms was observed, predominantly cyanobacteria (*Synechococcus* and *Prochlorococcus*) and, to a lesser extent, haptophytes and prasinophytes.

3.2 EOF-based analysis of the Rrs data

The spectral shapes and magnitude of the *in situ* hyperspectral Rrs are shown in Figure 08. In this figure, two distinct sets of water classes can be observed. One of them is characterized by a reflectance peak between 350 and 450 nm, in the violet and blue

wavelengths, a typical case of clear waters (Case 1 waters), where the water signal is predominant and there is a low optical contribution from phytoplankton (Mascarenhas & Keck, 2018). The second pattern, with a reflectance peak at 550 and 600 nm, within the green wavelength range, but with a less intense tail extending to 700 nm and the reduction in reflectance in the violet and blue spectrum, when compared to the spectra of clear water, suggests an optically more complex water (Case 2 water), where phytoplankton is the dominant signal and there are contributions from total suspended material (TSM) and colored dissolved organic matter (CDOM; Schalles, 2006).

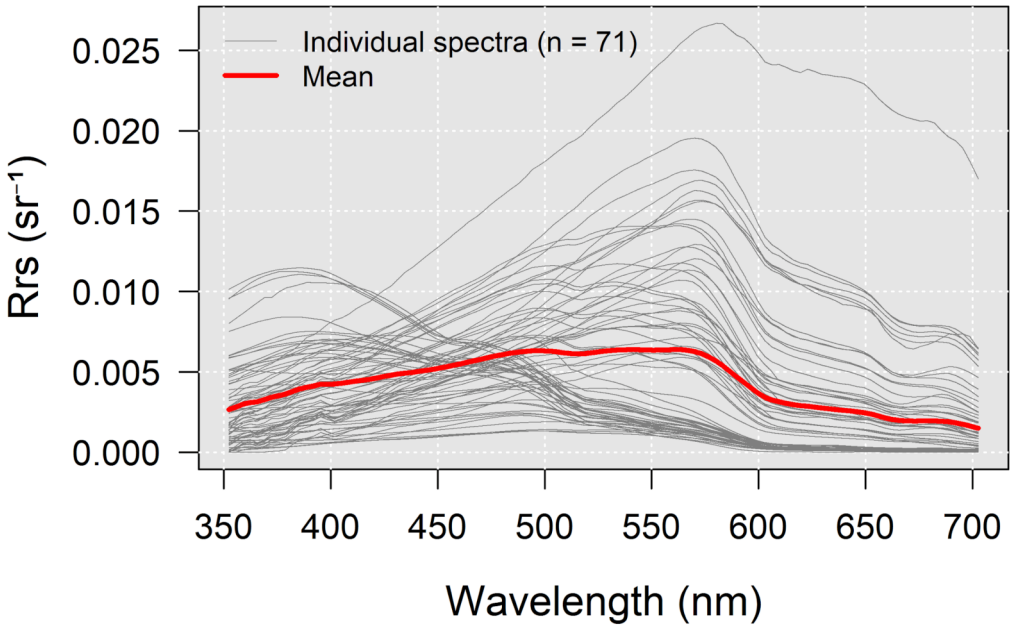


Figure 8. Remote sensing reflectance (Rrs) dataset. The grey lines indicate the spectral shapes and magnitude of each oceanographic station. The red line corresponding to the average spectra of the dataset.

These Rrs spectra were used to derive the significant EOF modes (Figure 09). Eight significant EOF modes were identified, with the first four modes accounting for 99.85% of the total variance. EOF1 accounts for approximately 79% of the variability in the dataset, indicating low reflectance in the ultraviolet wavelengths (eg. 350 nm), followed by absorption across the remaining wavelengths, suggesting a feature likely associated with the signal of pure water. EOF2 explains 16% of the total variability in the dataset, exhibiting a pronounced valley between 350 and 500 nm, which may indicate the influence of CDOM absorption in the violet and blue wavelengths, as well as a peak between 500 and 700 nm, indicative of reflectance from suspended particles

(phytoplankton and non-algal particles). EOF3 explains 3.5% of the observed variability, showing a peak between 425 and 575 nm, suggesting reflectance driven by some type of phytoplankton organisms and absorption of non-algal particles. EOF4 accounts for 0.8% of the variability, presenting two peaks, one between 400 and 550 nm and another between 625 and 700 nm, and a trough between 550 and 625 nm, indicating interactions associated with sets of accessory phytoplankton pigments. The remaining EOFs (EOF5, EOF6, EOF7, and EOF8) exhibit patterns that explain less than 0.1% of the variability.

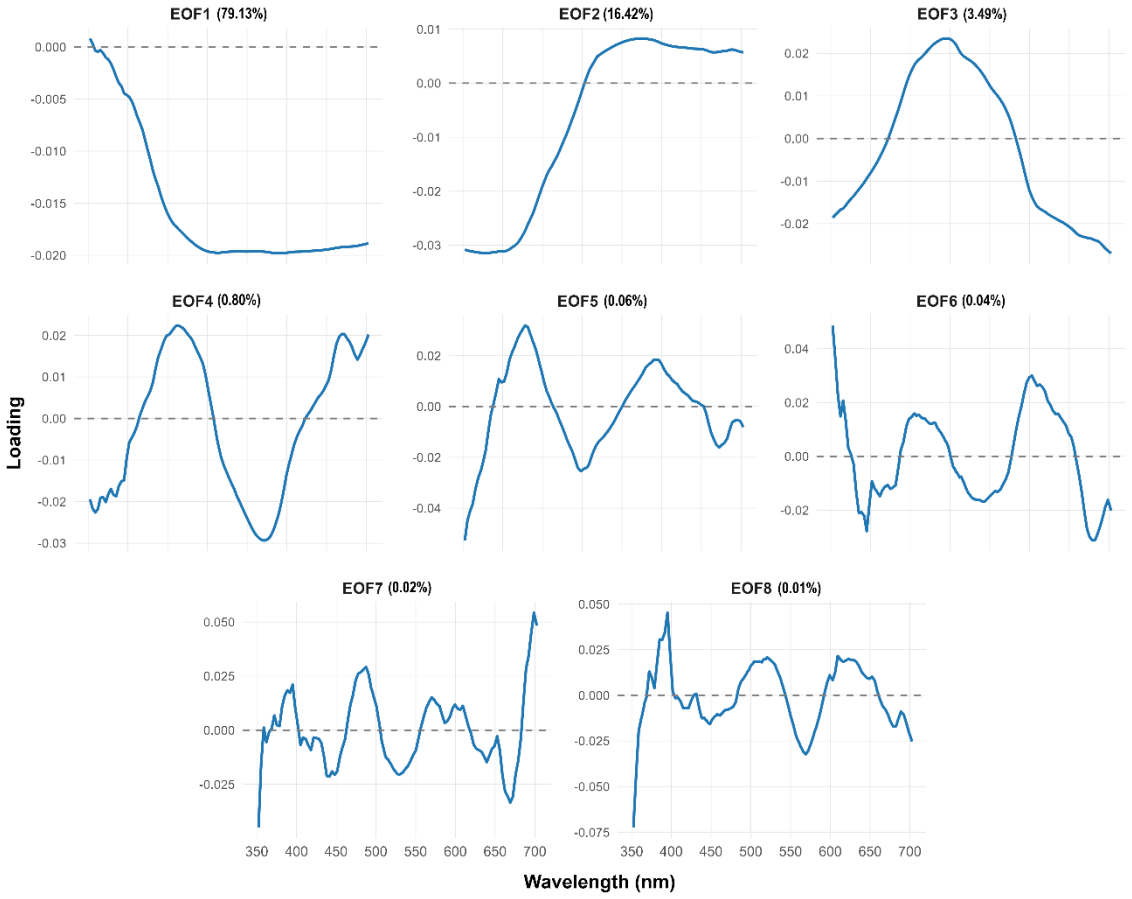


Figure 9. Distribution of the spectral loadings for the Empirical-Orthogonal Functions (EOF) modes derived from *in situ* hyperspectral remote sensing reflectance (Rrs) with their respective contribution (%) to the total variance.

3.3 PFT model evaluation

After the AIC selection, each PFT model was proposed (Table 02) as a linear regression with an intercept and regression coefficients for each EOF mode (as shown in Eq. 6). Each PFT employed between three and seven EOF modes, with *Synechococcus* being

the group that used the fewest EOFs in its formulation (e.g., EOF2, EOF6, and EOF8), whereas prasinophytes and cryptophytes used the greatest number (both excluding EOF7). EOF2 was the only component selected across all PFT models, suggesting that it likely captures the principal signal associated with phytoplankton, given both the proportion of explained variability and the optical component signatures it represents.

Table 2. Estimated intercepts and EOF-based regression coefficients for each phytoplankton functional type (PFT) model.

	Intercept	**EOF1**	**EOF2**	**EOF3**	**EOF4**	**EOF5**	**EOF6**	**EOF7**	**EOF8**
TChla	-0.2136	-0.0077	0.0117	—	-0.0522	—	-0.0399	0.1183	—
Pras	-1.4031	-0.0115	0.0235	0.0148	-0.0421	-0.0839	-0.1057	—	0.2219
Dia	-0.9218	-0.0110	0.0188	—	-0.0584	-0.0631	—	0.2038	-0.1745
Dino	-1.4965	-0.0088	0.0154	—	-0.0463	—	-0.0554	—	0.157
Hapt	-1.2025	-0.0033	0.0115	—	-0.0337	—	-0.1322	0.1275	0.1012
Cryp	-1.8208	-0.0174	0.0273	0.0132	-0.0870	-0.1367	-0.1269	—	0.2798
Syn	-1.0329	—	0.0040	—	—	—	-0.0711	—	0.0957
Proc	0.1747	-0.1058	0.0162	-0.2332	0.1901	—	—	0.8093	—

The model was evaluated by the regressions between TChla and PFTs Chla concentration determined by using HPLC-CHEMTAX (x‑axis) and the EOF‑based hyperspectral model prediction (y‑axis) (Figure 10). Although 71 oceanographic stations were obtained, with hyperspectral radiometric data and *in situ* PFTs, the number of concomitant samples for most groups varied because some groups were not detected in some stations. This is especially the case for *Prochlorococcus*, which was found in approximately half of the samples (n = 35). The full-fit correlation between in situ observed concentrations and those estimated by the EOF-based models for each PFT (Figure 10) demonstrated statistically significant agreement (p-value < 0.0001) for all groups.

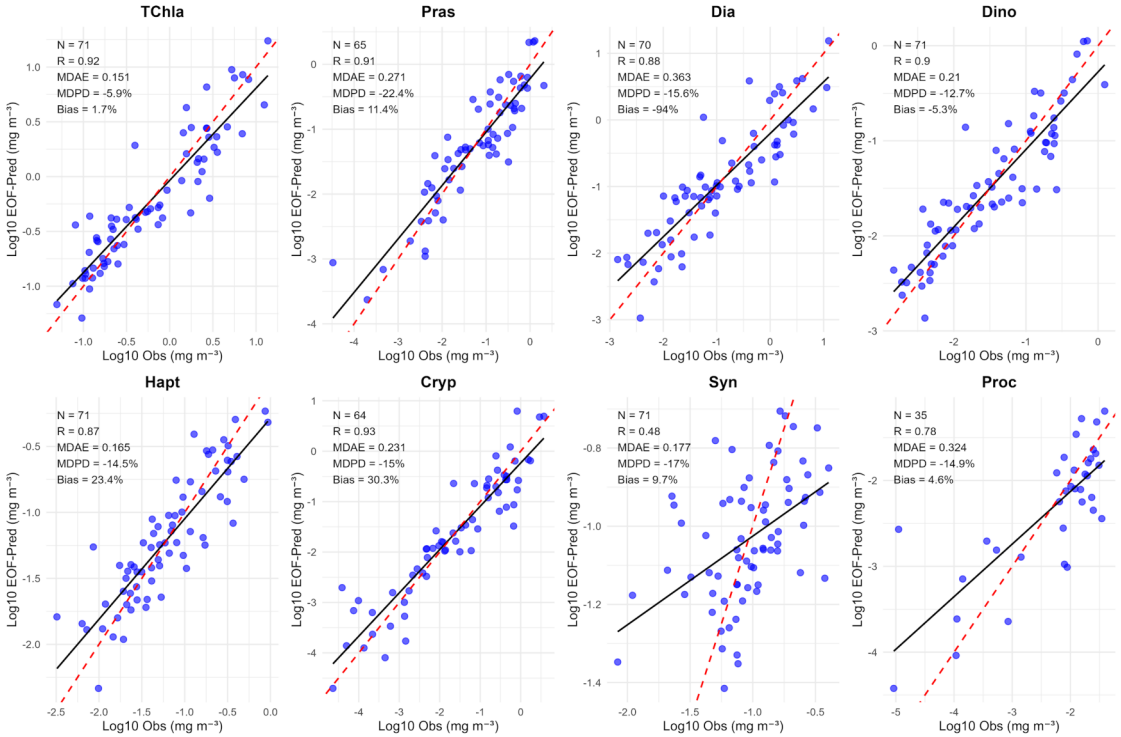


Figure 10. Regressions between TChla and PFT chlorophyll-a concentrations determined by HPLC-CHEMTAX (x-axis) and those predicted by the EOF-based hyperspectral model (y-axis). The linear regression fit is shown in black, while the 1:1 line is shown in red. Each blue point represents a matchup between model-estimated concentrations and in situ observations.

Pearson's correlation coefficients (Table 3) ranged from 0.48 to 0.93, indicating a strong positive linear relationship between the analysed variables for most PFTs. Only *Synechococcus* deviated, showing a moderate correlation (R = 0.48), deviating markedly from the pattern observed in the remaining groups. All other PFTs yielded correlations exceeding R = 0.70, including cryptophytes (R = 0.93), TChla (R = 0.92), dinoflagellates (R = 0.91), prasinophytes (R = 0.90), diatoms (R = 0.88), haptophytes (R = 0.87), and *Prochlorococcus* (R = 0.78), collectively indicating a consistent and robust linear association between the full fit measured variables for these groups.

TChla was identified as the best-performing model according to the error metrics, exhibiting the lowest bias and MDPD (Table 04). The negative MDPD values, ranging from –22.4% to –5.9%, indicate that the model systematically underestimates the concentrations of all analyzed phytoplankton groups, with median percent deviations between 6% and 22% below the observed values. Conversely, most bias metrics are positive, suggesting overestimation for the majority of samples or groups, only

dinoflagellates and diatoms showed underestimation. This divergence between metrics may suggest that the error distribution of the model is asymmetric. In this case, the use of MDPD may be smoothing the effects of this asymmetry, being more centered on the underestimation of PFT concentrations, while bias, as an absolute metric, may be influenced by a few samples that are overestimated by the model, generating large positive deviations. In the specific case of dinoflagellates and diatoms, both indicators converged to underestimation, suggesting that, in fact, the model underestimates at least these groups.

Table 3. Performance metrics for EOF-based models for Total Chlorophyll-a (TChla) and seven Phytoplankton Functional Types (PFTs), including Full-fit statistics and Cross-validation (cv) statistics.

	N	R	MDAE	MDPD	bias	Slope	R_cv	MDAE_cv	MDPD_cv	p-value
TChla	71	0.92	0.1508	-5.94	1.67	0.8411	0.90	0.1712	-6.36	2.89E-29
Pras	65	0.91	0.2711	-22.38	11.36	0.8233	0.76	0.3162	-24.87	2.13E-25
Dia	70	0.88	0.3625	-15.56	-93.99	0.7755	0.85	0.4211	-18.09	9.57E-24
Dino	71	0.90	0.2101	-12.68	-5.26	0.8161	0.88	0.2368	-13.81	4.45E-27
Hapt	71	0.87	0.1653	-14.47	23.36	0.7616	0.84	0.1946	-16.35	3.60E-23
Cryp	64	0.93	0.2315	-15.01	30.29	0.8588	0.84	0.3037	-15.30	4.84E-28
Syn	71	0.48	0.1770	-16.96	9.67	0.2269	0.37	0.1804	-18.20	2.68E-05
Proc	35	0.78	0.3239	-14.85	4.65	0.6127	0.66	0.4126	-19.91	2.77E-08

Cross‑validation statistics were used to evaluate the robustness of the TChla and PFTs fitted regression models (Table 04). All the statistical parameters obtained from the cross-validation procedure were comparable or slightly poorer than the full fit statics parameters. In general, Pearson correlation coefficient (R_cv) ranged from 0.37 to 0.9, where TChla was the best performer and *Synechococcus* was the worst. Most of the PFTs still maintained a high correlation, except cyanobacteria forms, *Prochlorococcus* and *Synechococcus*, which present medium (R = 0.66) and low correlation (R = 0.37), respectively. MDPDcv also showed some degree of underestimation, ranging from 6 to 24%, for TChla and all PFTs estimated, similarly to the full fit MDPD.

3.4 PFT model implementation on satellite data (PACE)

The EOF-based models were applied to an OCI/PACE imagery for March 20th 2025, in the SWAO continental shelf, to provide an example of the model application. The spatial maps were produced for TChla and all seven PFTs founded in this region (Figure 11).

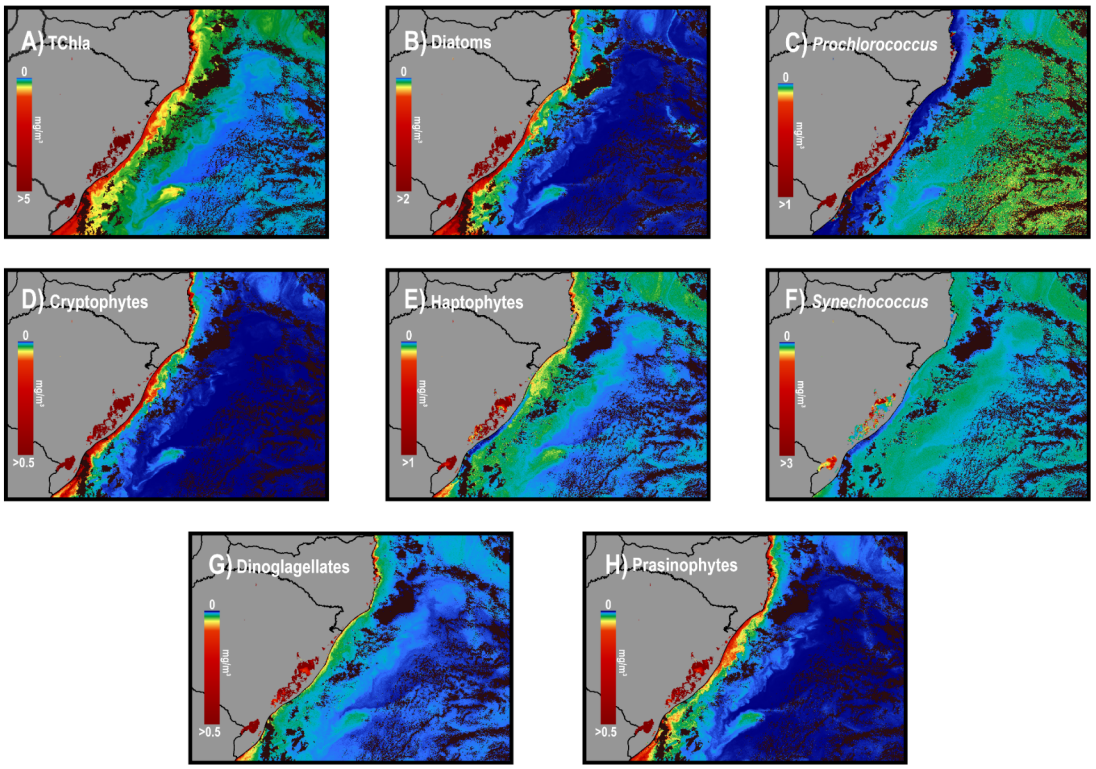


Figure 11. Spatial distribution of Total Chlorophyll-a (TChla, A), Diatoms (B), *Prochlorococcus* (C), Cryptophytes (D), Haptophytes (E), *Synechococcus* (F), Dinoglagellates (G) and Prasinophytes (H). These estimates were retrieved from Ocean Color Instrument (OCI) onboard NASA's Plankton, Aerosol, Cloud, ocean Ecosystem (PACE) from March 20th 2025. Dark grey areas in the maps show clouds. Each panel has its own color scale to highlight specific features of PFT biomass.

TChla exhibits higher concentrations in coastal regions closer to the continent, decreasing progressively with increasing distance offshore. A similar pattern, albeit less pronounced, is observed for diatoms, cryptophytes, haptophytes, dinoflagellates, and prasinophytes. In the case of Haptophytes and Dinoflagellates, despite their highest biomass occurring in proximity to the coast, they appear to exhibit a wider distribution extending into offshore waters. In contrast, cyanobacteria (*Synechococcus* and *Prochlorococcus*) display a more oceanic distribution, with *Prochlorococcus* confined to a zone farther from the coast, while *Synechococcus* shows a more homogeneous distribution across the image. The TChla distribution also reveals a filament-like offshore extension of higher phytoplankton biomass originating from the coastal zone, suggesting the advection of nutrient-enriched waters toward the open ocean. This feature is consistently observed in the distributions of diatoms, cryptophytes, haptophytes, dinoflagellates, and prasinophytes, but is absent in *Prochlorococcus*. Such

a pattern could indicate a localized nutrient enrichment driven by mesoscale or submesoscale processes (e.g., eddy activity and frontal dynamics), which promote the offshore transport of nutrient-rich coastal waters and enhance vertical mixing (Morales et al., 2017; Almeida et., 2025).

4. DISCUSSION

4.1 PFT modelling from hyperspectral Rrs in the SWAO coastal waters

In the coastal region under study, to date, there have been no studies that have developed, adapted, or calibrated remote sensing models for the estimation of PFTs using a chemotaxonomic approach, establishing the present study as a pioneering contribution in this regard. However, bio-optical models have been proposed for the remote estimation of phytoplankton size classes.

Notable among these is the model of Ciotti & Bricaud (2006), which proposed a bio-optical model to estimate a dominant phytoplankton size index. This model builds on previous analyses by Ciotti et al. (2002) and retrieves a spectral index of the dominant size class, related to variations in the phytoplankton absorption coefficient due to the packaging effect. This model was validated for the Brazilian continental shelf, which comprises optically complex Case 2 waters, using SeaWiFS data, with quite satisfactory results (Rudorff & Kampel, 2012). More recently, de Lima Oliveira et al. (2025) tested four approaches to estimate phytoplankton size classes from satellite data in the South Brazil Bight region. The models are based on the abundance method proposed by Brewin et al. (2010), which relates total chlorophyll-*a* concentration to the picoplankton, nanoplankton, and microplankton fractions through exponential functions. The study found that the most regionalized approach, which included SST data as a modelling parameter, yielded the best results for the South Brazil Bight region, as it incorporates an environmental driver into the allocation of biomass among phytoplankton size classes (de Lima Oliveira et al., 2025).

In respect to algorithms for functional groups specific to Brazilian coastal waters, studies are scarce. Rudorff & Kampel (2012), in a global review on remote sensing of PFTs, highlight that although models exist for coccolithophores (e.g., Brown & Yoder,

1994), *Trichodesmium* (e.g., Westberry et al., 2005), and diatoms (e.g., Sathyendranath et al., 2004), most were developed for other regions of the globe and have not been validated or calibrated for the Brazilian coast. Regarding pigment composition, Cunha et al. (2024) evaluated for the first time the applicability of ocean colour algorithms for functional groups in the Northeast region, initially applying the algorithm of El Hourany et al. (2019) to estimate six accessory pigments from GlobColour data. The authors indicated the feasibility of estimating dinoflagellates and haptophytes by satellite, albeit with limitations, especially for zeaxanthin estimation, due to the small *in situ* dataset and the need for more regional calibration.

In this context, the aim of this research was to accurately estimate TChla and phytoplankton community composition in coastal waters of the SWAO, an unprecedented effort for this region. This was achieved through the use of an approach adapted from Bracher et al. (2015), employing hyperspectral radiometric measurements applied to a coastal region of complex waters (Case-2 waters). Success was achieved ($R_cv \geq 0.7$ and p-value < 0.0001) in estimating TChla and five PFTs (diatoms, cryptophytes, dinoflagellates, haptophytes and prasinophytes), with moderate success for Prochlorococcus ($R_cv \geq 0.5$ and p-value < 0.0001), and systematic errors were found in the estimates for Synechococcus ($R_cv < 0.5$).

In general, EOF-based techniques for estimating cell abundance, pigment concentrations and PFTs Chla have been used with moderate success in the open ocean (Bracher et al., 2015; Xi et al., 2020) and in a few optically complex coastal regions (Craig et al., 2012; Vishnu et al., 2025). However, in these coastal regions with Case-2 waters, the Rrs signal, and consequently the EOF modes, is dominated not only by the absorption and scattering of water and phytoplankton, but also by other optical constituents such as CDOM, TSM and Non-Algal Particles (NAP; Kirk, 2010; Mascarenhas & Keck, 2018). Our study area, as described in section 2.1, is a dynamic oceanic region and is optically highly complex (Giannini et al., 2013). The influence of these components can be seen in the first three EOF modes (Figure 09), where these modes encompass the main optically active components of the water.

Empirical EOF-based models are intrinsically dependent on the quality, dynamic range, and spatio-temporal representativeness of the datasets used in their training and

validation phases. One of the most direct pieces of evidence for this dependence comes from the finding that the dynamic range of the target group concentrations in the training set directly determines the model's ability to predict extreme or rare values (Craig et al., 2012; Lange et al., 2020). This can lead to a series of effects, such as poor predictive performance for groups whose concentration range is narrow (Vishnu et al., 2025), failure to extrapolate to concentrations not represented in the training set (Craig et al., 2012), systematic underestimation of patch-distributed groups due to sparse sampling (Lange et al., 2020), loss of consistency in long-term time series due to lack of coverage of interannual variability and inter-sensor inconsistencies (Xi et al., 2023), dilution of signals from rare groups by spatial averaging (Vishnu et al., 2022), and reduced model robustness due to an insufficient number of matchups (Xi et al., 2020). Furthermore, empirical models such as those based on EOF require continuous recalibration to keep pace with climate-induced changes in phytoplankton assemblages, rendering them outdated and potentially biased if held static over time (Mouw et al., 2017).

In the regards of the bias metric (Table 03) diatoms stood out. Their bias reached -93%, which was substantially higher than that of the other PFTs. This happened because, at one specific oceanographic station, the observed diatom concentration was very close to 1 mg m^{-3} (0.9787 mg m^{-3}). When the logarithmic transformation was applied, values near 1 tended to zero.As the bias calculation (Eq. 9) involved a division by the observed value, which the denominator approached zero, and the bias metric became artificially inflated. Therefore, the high bias for diatoms does not necessarily reflect a disproportionately poor prediction, rather, it stems from a mathematical singularity arising from the combination of the logarithmic transformation and the structure of the bias metric.

The cyanobacterial genera (*Synechococcus* and *Prochlorococcus*) were the groups that exhibited the poorest performance among the PFTs proposed by the EOF-based models (Table 04), evidencing a recurring difficulty in estimating these organisms from hyperspectral Rrs measurements. Even in studies with global oceanic coverage, the retrieval of prokaryotes remains challenging (Xi et al., 2020), suggesting that the difficulty is inherent to the weak spectral signature of these groups at low surface

concentrations. This may be related to a number of different factors, among them the low magnitude and narrow range of the observed concentrations of these groups (Xi et al., 2020), thus constituting a limiting factor that may compromise the ability of EOF modes to extract pigments group-specific signals (Bracher et al., 2015).

The poor performance of our EOF-based models for *Synechococcus* and *Prochlorococcus* contrasts with the retrievals founded in the model Multiple Ordination ANAlysis (MOANA), proposed by Lange et al. (2020) and offered as one of the provisional level 4 products of OCI/PACE (NASA, 2025b). MOANA was developed using a training dataset that covered a broad trophic gradient across the Atlantic Ocean, to set up regression models based on Rrs, flow cytometry cell counts, and sea surface temperature (SST), in order to estimate surface abundances of *Prochlorococcus*, *Synechococcus*, and autotrophic picocukaryotes in open ocean. MOANA training dataset covered from extensive oligotrophic gyres to mesotrophic high latitudes, where cyanobacteria forms dominate and strongly influence the optical signal (Flombaum et al., 2013; Lange et al., 2020). In contrast, the model proposed by the current research focused on coastal waters, where CDOM, TSM and NAP modify the magnitude and shape of the Rrs spectrum.

Another factor that may be related to this limiting performance in estimating these groups is the fact that sea surface temperature (SST) was not included as a covariate in the proposed models, but was included in MOANA. This variable is extremely important because it is a constraint on the distribution of these cyanobacteria groups (Flombaum et al., 2013) and acts as a proxy for water-column stratification, a fundamental condition for the development of *Prochlorococcus* in oligotrophic environments (Bouman et al., 2003; 2006). This suggests that incorporating SST as an additional covariate in our models could potentially enhance their performance for cyanobacteria, particularly *Prochlorococcus*, by accounting for the thermal and stratification niches that favor these groups.

Additionally, zeaxanthin, one of the marker pigments for cyanobacterial groups, has shown weaker retrievals, particularly in environments where its concentration is low (Bracher et al., 2015; Chase et al., 2017). This points to an inherent limitation of surface remote sensing estimates for these groups when the model is based on pigment

composition and/or chemotaxonomic groups. Although zeaxanthin is a reliable indicator of cyanobacterial biomass, this pigment is not exclusive to the cyanobacterial lineage, as its presence in multiple co-occurring genera could prevent the accurate discrimination between ecologically distinct groups (Pniewski, 2020; Sugiyama & Takaichi, 2020). Furthermore, the concentration of zeaxanthin is not static, it is dynamically regulated by the xanthophyll cycle, increasing markedly under high light (Pniewski, 2020; Giossi, 2025). This physiological variability can decouple zeaxanthin concentration from actual cyanobacterial biomass, introducing additional uncertainty into remote sensing pigments-based retrievals.

It also suggests that an approach similar to that of Lange et al. (2020), which relies on cell abundances rather than PFT Chla, could serve as an alternative for the remote estimation of cyanobacteria in coastal waters. Although MOANA was not directly developed for coastal environments, the authors explicitly state that the models could be retuned for such waters to account for the effects of CDOM, TSM and NAP on the spectral signature (Lange et al., 2020). Therefore, the two methodologies can be seen as complementary and, acting synergistically, would enable a more precise and accurate description of phytoplankton groups at the sea surface from ocean color remote sensing measurements.

Despite the challenges in retrieving cyanobacteria groups, the model successfully captured expected spatial patterns of PFT distribution, as illustrated in the PACE image from 20 March 2025. Furthermore, the spatial EOF-derived phytoplankton composition maps for 20 March 2025 revealed a decreasing TChla gradient from the coast toward the open ocean, with diatoms, cryptophytes, haptophytes, dinoflagellates and prasinophytes following a similar pattern, whereas cyanobacteria exhibited a more typically oceanic distribution. In this regard, this first example revealed spatial PFT distribution patterns that are consistent with the established oceanographic knowledge for this region of the southwestern Atlantic (e.g., Islabão et al., 2017; Brandini, 2018; Giannini et al., 2021; Bueno et al., 2025), and are further corroborated by the *in situ* findings described in section 3.1. These observations represent the first evidence that the proposed models are applicable and may be suitable for use with hyperspectral remote sensing data in the region.

Notably, the image also captured a filament-like offshore extension, presented in section 3.4, detected in all groups except *Prochlorococcus*. This is an interesting feature, as this biomass extension may indicate the influence of processes associated with the Brazil-Malvinas Confluence, where a system of mesoscale eddies and frontal instabilities can promote the export of colder, nutrient-rich shelf waters into the open ocean, a process that extends its influence northward to approximately 32-33°S (Berden et al., 2020). Such processes favor phytoplankton groups that depend on greater nutrient availability, in contrast to cyanobacteria, which are adapted to oligotrophic conditions (Carvalho et al., 2022).

Despite the ecological coherence of the patterns obtained, the PACE image also revealed important limitations of the models. Figure 11 reveals a saturation of PFTs biomass in inland waters, for which the models were not trained to provide reliable estimates. A second saturation pattern is observed in the *Prochlorococcus* distribution, where the nearshore region, where this group is not expected to occur, is characterized by apparent supersaturation. This type of misassignment in high-chlorophyll areas has already been documented for reflectance-based algorithms, which tend to overestimate picocyanobacteria in eutrophic coastal environments (Correa-Ramirez et al., 2018). Such artefacts arise largely from extrapolating the model to optical and biogeochemical conditions not represented in the training dataset, especially when the dynamic range of the calibration data is insufficient for groups with low biomass contribution (Craig et al., 2012; Vishnu et al., 2025). This suggests potential instability in the model when handling concentrations near zero.

To overcome this limitation, we recommend restructuring the original model by incorporating new training samples, especially for *Prochlorococcus* and *Synechococcus*, prioritizing points where these groups exhibit a dominant signal or higher concentrations, thereby expanding the model's dynamic range and reducing saturation artefacts in shallow coastal environments (Xi et al., 2020). These improvements, together with extensive validation of the proposed models applied to OCI/PACE products and other hyperspectral platforms, will be essential to consolidate remote PFT estimates in the region, with independent validation using *in situ* pigment composition

data or new field campaigns representing an indispensable step in this process (Soja-Woźniak et al., 2017; Mouw et al., 2017).

4.2 PFT distribution in the SWAO coast and its ecological and biogeochemical impacts

The phytoplankton groups estimated in this study (diatoms, dinoflagellates, haptophytes, prasinophytes, cryptophytes, *Synechococcus* and *Prochlorococcus*) play distinct and complementary roles in marine biogeochemical cycles, and that's one of the reasons why is so important to have a way to estimate PFTs with high spatiotemporal resolution on ocean surface. In addition to having different relationships with biogeochemical cycles, PFTs serve as robust indicators of ecosystem functioning and represent essential tools for climate and ecological modelling (Le Quéré et al., 2005; Dutkiewicz et al., 2020). In the SWAO, the *in situ* surface distribution of these groups followed clear latitudinal and zonal patterns, modulated by regional oceanographic features (Figure 7).

At lower latitudes, phytoplankton biomass was lower, driven by prevailing meteorological and oceanographic conditions (eg., notably higher temperatures and the oligotrophic nature of the dominant water masses). These conditions favoured the development of smaller PFTs, particularly picoplanktonic cyanobacteria and haptophytes (Brandini, 2018; Carvalho et al., 2022). Nevertheless, two notable exceptions were observed within the 20–25°S latitudinal band, close to stations 80a and 80c near Cabo de São Tomé, as well as stations 70 and 71 near the mouth of the Paraíba do Sul River (Figure 7f). These stations exhibited higher phytoplankton biomass and diversity than adjacent sites at similar latitudes. Such deviations are consistent with local processes documented in the region. An eddy-induced upwelling system is known near Cabo de São Tomé, associated with quasi-stationary cyclonic meanders of the BC, whic can lift nutrient-rich SACW onto the continental shelf, promoting surface divergence and increasing nutrient availability (Calado et al., 2010; Almeida et al., 2025). Concurrently, the freshwater discharge of the Paraíba do Sul River introduces low-salinity, silicate-rich coastal water, which may enhance phytoplankton biomass and favour a more diverse community, including diatoms and certain dinoflagellates (Moser et al., 2014).

Figure 7 also reveals a clear differentiation in community structure along the coast-offshore axis, pointed on section 3.1. At stations closest to the coastline, characterised by greater physical turbulence and higher continental nutrient inputs, diatoms predominated overwhelmingly, followed by minor contributions from cryptophytes and dinoflagellates (Islabão et al., 2017; Brandini, 2018). From a biogeochemical perspective, the dominance of diatoms near the coast implies a tight coupling of the carbon and silica cycles, as their siliceous frustules enhance sinking and organic carbon export (Tréguer et al., 2018). Cryptophytes, though less abundant, contribute to carbon transfer within the microbial food web and are efficient grazer food (Qu et al., 2024). Dinoflagellates, even in low proportions, are relevant because many species are mixotrophic and some can form harmful algal blooms, which can cause a range of dermatological, hepatic, and neurological effects on the biota (Hamdan et al., 2017; Calbet, 2025).

Moving towards the outer shelf and slope, a gradual replacement of these coastal groups by picoplanktonic forms was observed, with cyanobacteria (*Synechococcus* and *Prochlorococcus*) becoming dominant, accompanied by smaller contributions from haptophytes and prasinophytes (Islabão et al., 2017). This pattern is a direct consequence of the shift from a well-mixed, nutrient-replete coastal regime to a stratified, oligotrophic regime offshore, where small-celled organisms with high surface-to-volume ratios are better adapted to low nutrient availability (Brandini, 2018; Lima et al., 2019). In this oligotrophic regime, cyanobacteria have low sinking rates, so their biomass is largely recycled in surface waters, sustaining the microbial loop in the oceanic region (Ger et al., 2014). Moreover, some cyanobacteria are diazotrophic, capable of fixing atmospheric nitrogen, which directly influences the nitrogen cycle and confers a competitive advantage in oligotrophic waters (Brandini, 2018). Haptophytes, though present in lower biomass in the same offshore waters, also exhibit distinct biogeochemical traits linked to their oceanic distribution. Their calcifying species produce coccoliths that enhance ballast but simultaneously release CO_2 during calcification, affecting the carbon cycle (Eikrem et al., 2016); conversely, non-calcifying haptophytes produce dimethylsulfoniopropionate (DMSP), contributing to the marine sulfur cycle (Thomsen et al., 1994; Liu et al., 2009).

The clear differentiation along latitudinal and coast-offshore gradients in PFT distribution reinforces the strong influence of regional oceanographic features on phytoplankton community structure (Brandini, 2018; Carvalho et al., 2022). The distinct biogeochemical roles played by each group underscore the relevance of resolving PFTs for understanding marine ecosystem functioning and biogeochemical fluxes (IOCCG, 2014; Chase et al., 2022; Li et al., 2023). Therefore, the ability to estimate PFTs from satellite remote sensing represents a critical step towards improving ecological and climate models in this dynamic and optically complex ocean region.

4.3 Future prospects for PFT estimates on hyperspectral sensors

The future of hyperspectral RS data is extremely promising, particularly with regard to the discrimination of PFTs. This is because the new spectral resolution, spanning to all across the visible radiation, represents a leap forward compared to traditional multispectral sensors (e.g., MODIS, VIIRS, MERIS, Sentinel-3), enabling the capture of subtle spectral features associated with accessory pigments, fluorescence, and particle scattering (Bracher et al., 2017; Cetinić et al., 2024). Nevertheless, despite significant advances, challenges remain when working with these hyperspectral data, particularly in the atmospheric correction process, *in situ* validation, and algorithm transferability, which must be overcome before remote estimates of PFTs reach their full potential.

PRISMA is a hyperspectral sensor and has been tested in inland and coastal waters for more general retrievals, such as TSM, CDOM, and Chla (Niroumand-Jadidi et al., 2020; Bresciani et al., 2022), but also for specific phytoplankton pigments such as phycocyanin (Lima et al., 2023). However, despite results showing good agreement with *in situ* data, discrepancies related to glint effect and atmospheric correction have been observed, especially in the blue bands (Niroumand-Jadidi et al., 2020). Pellegrino et al. (2023) suggested that this limitation could be due to the fact that the standard PRISMA products processor was designed for terrestrial applications. Atmospheric correction also poses a challenge for EnMAP data, exhibiting underestimation of water reflectance and spectral noise at wavelengths below 450 nm, in addition to being optimized for clear waters (Soppa et al., 2024).

The OCI/PACE reflectance data used in this study to estimate PFTs from space are provisional Level-2 products processed with the standard heritage atmospheric correction algorithm (Werdell et al., 2024; NASA, 2025a). Although effective in open oceans, this algorithm has known limitations in optically complex coastal waters, as it does not handle absorbing aerosols well, ignores non-zero water reflectance in the near-infrared, and suffers from adjacency and sun glint effects (Frouin et al., 2019). These uncertainties may affect the EOF model estimates, especially in coastal regions with high CDOM and TSM loads. In addition to the intrinsic limitations of the EOF models, the quality of the input reflectance data is also affected by the applied atmospheric correction method. To circumvent these limitations, we recommend testing alternative processors such as POLYMER (Steinmetz et al., 2011; Steinmetz & Ramon, 2018) or ACOLITE (Vanhellemont & Ruddick, 2016; Vanhellemont & Ruddick, 2018). Future studies may compare the effect of different atmospheric corrections on the EOF-based PFT estimates presented in this work.

With regard to phytoplankton composition and PFTs, the MOANA (Multiple Ordination ANAlysis) algorithm has been implemented on a provisional basis for OCI/PACE operational processing stream and provides cell abundance estimates of *Prochlorococcus*, *Synechococcus* and autotrophic picoeukaryotes (Lange et al., 2020; NASA, 2025b). In addition to MOANA, the scientific community has developed experimental approaches that more broadly exploit the hyperspectral capability. HyperPFT, for example, uses an ensemble of Transformer networks trained on a dataset expanded by spectral reconstruction via a Generative Adversarial Network, allowing the estimation of eight functional groups and providing per-pixel uncertainty (Zhang et al., 2026). The XGBoost-based model employs decision trees and Shapley Additive Explanations analysis, achieving high accuracy for diatoms, cyanobacteria and coccolithophores, although with lower performance for dinoflagellates (Craig & Karaköylü, 2025). In this sense, the present study joins other research groups in breaking new ground, seeking to accurately estimate PFTs from space.

5. CONCLUSION

The results demonstrate that phytoplankton biomass and composition in the Southwestern Atlantic are strongly regulated by environmental gradients operating

across multiple scales. A consistent latitudinal pattern was observed, with lower Chla concentrations at lower latitudes, associated with warmer, oligotrophic waters that favor small-sized organisms such as cyanobacteria. However, relevant local deviations, such as those observed near Cabo de São Tomé and at the mouth of the Paraíba do Sul River, in the Southeastern coast, indicate that regional processes, including upwelling induced by meanders of the Brazil Current and fluvial input, can enhance nutrient availability and promote more diverse and productive communities. This finding underscores the importance of the interactions between mesoscale physical forcing and coastal processes in structuring phytoplankton communities.

Along the coast–ocean gradient, the data reveal a clear replacement of functional groups, reflecting changes in the physicochemical properties of the water. Coastal regions, characterized by higher turbulence and nutrient availability, were dominated by diatoms, whereas stratified oceanic areas favored the dominance of picoplankton, particularly cyanobacteria. This pattern was consistent across both *in situ* observations and model-derived estimates, indicating that phytoplankton community variability can be interpreted as a predictable ecological response to environmental conditions. Furthermore, spectral analysis based on EOF proved effective in capturing the main optical components of the water column, clearly distinguishing between Case 1 and Case 2 waters and highlighting the dominant role of constituents such as phytoplankton, CDOM, and TSM in modulating the optical signal.

EOF-based models exhibited robust performance for most functional groups and for TChla, with high correlations and statistical significance, confirming the potential of this approach for applications in optically complex coastal waters. Nevertheless, the presence of systematic errors, particularly the generalized underestimation and the poorer performance for cyanobacteria, reveals important limitations. These limitations are associated with both the low representativeness of these groups in the training dataset and their weak spectral signature at low concentrations, as well as the absence of relevant environmental variables such as sea surface temperature. Discrepancies among error metrics also suggest asymmetric residual distributions, emphasizing the need for careful evaluation of the statistical indicators employed.

Finally, the application of the models to PACE satellite data demonstrated their ability to reproduce ecologically consistent spatial patterns, such as the coastal–ocean gradient and the offshore export of biomass in the form of filaments associated with mesoscale processes. For the first time in the SAWO region, we provide unprecedented evidence of these patterns based on a regional bio-optical model. However, it also revealed significant limitations related to extrapolation under conditions not represented in the training dataset, such as saturation effects in coastal waters and the overestimation of *Prochlorococcus* nearshore. These results suggest that, although promising, the approach requires further refinement, including the expansion of calibration datasets, improved representation of rare groups, and testing with different atmospheric correction algorithms. Overall, this study represents a significant advancement in the remote estimation of phytoplankton functional types, while also clearly delineating the challenges that must be addressed for more reliable operational applications.

ACKNOWLEDGEMENTS

The authors would like to thank the officers and crew of the vessels Lancha Larus, Veleiro ECO, and NOc. Atlântico Sul for the opportunity to perform sampling in the SWAO region. We are also grateful to all those involved in the process of obtaining and collecting the PFT and radiometric samples. This work was funded by Conselho Nacional de Desenvolvimento Científico e Tecnológico (CNPq), through the projects MCT-II (), INCT-Mar COI (400551/2014-4), CNPq Edital Universal (406502/2021-8) and Rede Nacional de Observação e Monitoramento Oceânico ReNOMO (409666/2022-0). N. Heinz received a scholarship from Coordenação de Aperfeiçoamento de Pessoal de Nível Superior (CAPES, process number 88887.948831/2024-00).

REFERENCES

Almeida, I. R., de Amorim, J. P. M., Souza-Neto, P. W. M. E., & da Silveira, I. C. A. (2025). On the propagation and surface chlorophyll-a signature of long-lived Brazil Current eddies. Ocean Dynamics, 75(8), 72.

Alvain, S., Moulin, C., Dandonneau, Y., & Breon, F. M. (2005). Remote sensing of phytoplankton groups in case 1 waters from global SeaWiFS imagery. Deep Sea Research Part I: Oceanographic Research Papers, 52(11), 1989-2004.

Berden, G., Charo, M., Möller Jr, O. O., & Piola, A. R. (2020). Circulation and hydrography in the western South Atlantic shelf and export to the deep adjacent ocean: 30 S to 40 S. Journal of Geophysical Research: Oceans, 125(10), e2020JC016500.

Bouman, H. A., Platt, T., Sathyendranath, S., Li, W. K., Stuart, V., Fuentes-Yaco, C., ... & Kyewalyanga, M. (2003). Temperature as indicator of optical properties and community structure of marine phytoplankton: implications for remote sensing. Marine Ecology Progress Series, 258, 19-30.

Bouman, H. A., Ulloa, O., Scanlan, D. J., Zwirglmaier, K., Li, W. K., Platt, T., ... & Sathyendranath, S. (2006). Oceanographic basis of the global surface distribution of Prochlorococcus ecotypes. Science, 312(5775), 918-921.

Bracher, A., Taylor, M. H., Taylor, B., Dinter, T., Roettgers, R., & Steinmetz, F. (2015). Using empirical orthogonal functions derived from remote-sensing reflectance for the prediction of phytoplankton pigment concentrations. Ocean Science, 11(1), 139-158.

Bracher, A., Xi, H., Dinter, T., Mangin, A., Strass, V., Von Appen, W. J., & Wiegmann, S. (2020). High resolution water column phytoplankton composition across the Atlantic Ocean from ship-towed vertical undulating radiometry. Frontiers in Marine Science, 7, 235.

Brandini, F. P. (2018). Phytoplankton assemblages of the subtropical South West Atlantic: Composition and dynamics in relation to physical and chemical processes. In M. S. Hoffmeyer, M. E. Sabatini, F. P. Brandini, D. L. Calliari, & N. H. Santinelli (Eds.), Plankton ecology of the Southwestern Atlantic: From the subtropical to the Subantarctic realm (pp. 129–148). Springer. https://doi.org/10.1007/978-3-319-77869-3_7.

Bresciani, M., Giardino, C., Fabretto, A., Pellegrino, A., Mangano, S., Free, G., & Pinardi, M. (2022). Application of new hyperspectral sensors in the remote sensing of aquatic ecosystem health: Exploiting PRISMA and DESIS for four Italian lakes. Resources, 11(2), 8.

Brewin, R. J., Sathyendranath, S., Hirata, T., Lavender, S. J., Barciela, R. M., & Hardman-Mountford, N. J. (2010). A three-component model of phytoplankton size class for the Atlantic Ocean. Ecological Modelling, 221(11), 1472-1483.

Brewin, R. J., Ciavatta, S., Sathyendranath, S., Jackson, T., Tilstone, G., Curran, K., et al. & Raitsos, D. E. (2017). Uncertainty in ocean-color estimates of chlorophyll for phytoplankton groups. Frontiers in Marine Science, 4, 104.

Brotas, V., Ferreira, A., Veloso, V., Tracana, A., Guerreiro, C. V., Tarran, G. A., et al. & Groom, S. B. (2023). Assessing phytoplankton community composition in the Atlantic Ocean from in situ and satellite observations. Frontiers in Marine Science, 10, 1229692.

Brown, C. W., & Yoder, J. A. (1994). Coccolithophorid blooms in the global ocean. Journal of Geophysical Research: Oceans, 99(C4), 7467-7482.

Bueno, J. V. L., Kerr, R., de Oliveira Carvalho, A. D. C., & Mendes, C. R. B. (2025). The role of phytoplankton in the deep chlorophyll maximum CO2 dynamics along a

zonal section (34.5° S) in South Atlantic Ocean. Marine Environmental Research, 210, 107314.

Calado, L., da Silveira, I. C. A., Gangopadhyay, A., & de Castro, B. M. (2010). Eddy-induced upwelling off Cape São Tomé (22°S, Brazil). Continental Shelf Research, 30(10–11), 1181–1188.

Calbet, A. (2025). On the ecological duality between ciliates and dinoflagellates across marine ecosystems. Journal of Plankton Research, 47(5), 1–16.

Campos, P. C., Möller Jr, O. O., Piola, A. R., & Palma, E. D. (2013). Seasonal variability and coastal upwelling near Cape Santa Marta (Brazil). Journal of Geophysical Research: Oceans, 118(3), 1420-1433.

Canuti, E., Artuso, F., Bracher, A., Brotas, V., Devred, E., Dimier, C., Giardina, I., Mendes, C.R.B., Murawski, S., Peeken, I., Tracana, A., Ras, J., Wiegmann, S., (2022). The Fifth HPLC Intercomparison on Phytoplankton Pigments (HIP-5). Publications Office of the European Union, Luxembourg.

Carvalho, A. C. O., Kerr, R., Tavano, V. M., & Mendes, C. R. B. (2022). The southwestern South Atlantic continental shelf biogeochemical divide. Biogeochemistry, 159(2), 139-158. https://doi.org/10.1007/s10533-022-00918-8.

Chase, A. P., Boss, E., Cetinić, I., & Slade, W. (2017). Estimation of phytoplankton accessory pigments from hyperspectral reflectance spectra: toward a global algorithm. Journal of Geophysical Research: Oceans, 122(12), 9725-9743.

Chase, A. P., Boss, E., Haentjens, N., Culhane, E., Roesler, C., & Karp-Boss, L. (2022). Plankton imagery data inform satellite-based estimates of diatom carbon. Geophysical Research Letters, 49, e2022GL098076.

Ciotti, A. M., Odebrecht, C., Fillmann, G., & Möller, O. O., Jr. (1995). Freshwater outflow and Subtropical Convergence influence on phytoplankton biomass on the southern Brazilian continental shelf. Continental Shelf Research, 15(14), 1737–1756.

Ciotti, A. M., Lewis, M. R., & Cullen, J. J. (2002). Assessment of the relationships between dominant cell size in natural phytoplankton communities and the spectral shape of the absorption coefficient. Limnology and Oceanography, 47(2), 404-417.

Ciotti, A. M., & Bricaud, A. (2006). Retrievals of a size parameter for phytoplankton and spectral light absorption by colored detrital matter from water-leaving radiances at SeaWiFS channels in a continental shelf region off Brazil. Limnology and Oceanography: Methods, 4(7), 237–253.

Correa-Ramirez, M., Morales, C. E., Letelier, R., Anabalón, V., & Hormazabal, S. (2018). Improving the remote sensing retrieval of phytoplankton functional types (PFT) using empirical orthogonal functions: A case study in a coastal upwelling region. Remote Sensing, 10(4), 498.

Craig, S. E., Jones, C. T., Li, W. K., Lazin, G., Horne, E., Caverhill, C., & Cullen, J. J. (2012). Deriving optical metrics of coastal phytoplankton biomass from ocean colour. Remote Sensing of Environment, 119, 72-83.

Craig, S. E., & Karaköylü, E. M. (2025). Phytoplankton community composition retrieval from space. ESS Open Archive. https://doi.org/10.22541/essoar.175433969.93496022/v1.

Cunha, E. V., de Castro Melo, P. A. M., Farias, G. B., and Vantrepotte, V.: Assessment of Phytoplankton Biomass and Diversity in Northeast Brazil via Satellite Ocean Color Observation (2024). Int. Arch. Photogramm. Remote Sens. Spatial Inf. Sci., XLVIII-3-2024, 89–95, https://doi.org/10.5194/isprs-archives-XLVIII-3-2024-89-2024.

Cury, P. M., Shin, Y. J., Planque, B., Durant, J. M., Fromentin, J. M., Kramer-Schadt, S., ... & Grimm, V. (2008). Ecosystem oceanography for global change in fisheries. Trends in Ecology & Evolution, 23(6), 338-346.

Cusick, K. D., & Widder, E. A. (2020). Bioluminescence and toxicity as driving factors in harmful algal blooms: Ecological functions and genetic variability. Harmful Algae, 98, 101850.

de Lima Oliveira, A., Rudorff, N., Sathyendranath, S., Dall Cortivo, F., Vianna Rodrigues, S., Sudatti, D., ... & Kampel, M. (2025). Advancing regional satellite-based assessment of phytoplankton size structure in a subtropical Bight. International Journal of Remote Sensing, 46(22), 8784-8819.

Dominguez, J. M. (2009). The coastal zone of Brazil. In Geology and geomorphology of holocene coastal barriers of Brazil (pp. 17-51). Berlin, Heidelberg: Springer Berlin Heidelberg.

Dutkiewicz, S., Cermeno, P., Jahn, O., Follows, M. J., Hickman, A. E., Taniguchi, D. A., & Ward, B. A. (2020). Dimensions of marine phytoplankton diversity. Biogeosciences, 17(3), 609-634.

Eikrem, W., Medlin, L. K., Henderiks, J., Rokitta, S., Rost, B., Probert, I., Throndsen, J., & Edvardsen, B. (2016). Haptophyta. In J. M. Archibald, A. G. B. Simpson, & C. H. Slamovits (Eds.), Handbook of the Protists (2nd ed., pp. 1–61). Springer.

El Hourany, R., Abboud‐abi Saab, M., Faour, G., Aumont, O., Crépon, M., & Thiria, S. (2019). Estimation of secondary phytoplankton pigments from satellite observations using self‐organizing maps (SOMs). Journal of Geophysical Research: Oceans, 124(2), 1357-1378.

Falkowski, P. G. (1994). The role of phytoplankton photosynthesis in global biogeochemical cycles. Photosynthesis research, 39: 235-258.

Fargion, G. S., & Mueller, J. L. (Eds.). 2000. Ocean Optics Protocols for Satellite Ocean Color Sensor Validation, Revision 2 (NASA/TM-2000-209966). NASA Goddard Space Flight Center.

Field, C. B.; Behrenfeld, M. J.; Randerson, J. T.; & Falkowski, P. (1998). Primary production of the biosphere: integrating terrestrial and oceanic components. Science, 281(5374): 237-240.

Flombaum, P., Gallegos, J. L., Gordillo, R. A., Rincón, J., Zabala, L. L., Jiao, N., ... & Martiny, A. C. (2013). Present and future global distributions of the marine Cyanobacteria Prochlorococcus and Synechococcus. Proceedings of the National Academy of Sciences, 110(24), 9824-9829.

Franke, J., Heinzel, V., & Menz, G. (2006, July). Assessment of NDVI-differences caused by sensor specific relative spectral response functions. In 2006 IEEE International Symposium on Geoscience and Remote Sensing (pp. 1138-1141). IEEE.

Franz, G., Garcia, C. A., Pereira, J., de Freitas Assad, L. P., Rollnic, M., Garbossa, L. H. P., ... & Polejack, A. (2021). Coastal ocean observing and modeling systems in Brazil: initiatives and future perspectives. Frontiers in Marine Science, 8, 681619.

Frouin, R. J., Franz, B. A., Ibrahim, A., Knobelspiesse, K., Ahmad, Z., Cairns, B., ... & Zhai, P. W. (2019). Atmospheric correction of satellite ocean-color imagery during the PACE era. Frontiers in earth science, 7, 145.

Garcia, C. A. E., Garcia, V. M. T., & McClain, C. R. (2005). Evaluation of SeaWiFS chlorophyll algorithms in the Southwestern Atlantic and Southern Oceans. Remote Sensing of Environment, 95(1), 125-137.

Garcia, C. A., & Garcia, V. M. (2008). Variability of chlorophyll-a from ocean color images in the La Plata continental shelf region. Continental Shelf Research, 28(13), 1568-1578.

Garver, S. A., Siegel, D. A., & B. Greg, M. (1994). Variability in near‐surface particulate absorption spectra: What can a satellite ocean color imager see?. Limnology and Oceanography, 39(6), 1349-1367.

Ger, K. A., Hansson, L. A., & Lürling, M. (2014). Understanding cyanobacteria–zooplankton interactions in a more eutrophic world. Freshwater Biology, 59(9), 1783–1798.

Giannini, M. F. C., Garcia, C. A. E., Tavano, V. M., & Ciotti, Á. M. (2013). Effects of low-salinity and high-turbidity waters on empirical ocean alcolour gorithms: an example for Southwestern Atlantic waters. Continental Shelf Research, 59, 84-96.

Giannini, F., Mendes, C. R. B., Garcia, C. A. E., Carvalho, A. C. O., & Ciotti, A. M. (2021). Phytoplankton community and the fluorescence-derived photo-physiological parameters in the South Atlantic Ocean. Journal of Marine Systems, 218, 103538.

Giossi, C. E. (2025). Xanthophyll cycle dynamics in the model diatom Phaeodactylum tricornutum: molecular characterisation and combined effects of temperature and light. Doctoral thesis, University of Konstanz, Germany.

Gonçalves-Araujo, R., de Souza, M. S., Tavano, V. M., Mendes, C. R., de Souza, R. B., Schultz, C., & Pollery, R. C. (2018). Phyto-and protozooplankton assemblages and

hydrographic variability during an early winter survey in the Southern Brazilian Continental Shelf. Journal of Marine Systems, 184, 36-49.

Guimaraens, M. A., & Coutinho, R. (1996). Spatial and temporal variation of benthic marine algae at the Cabo Frio upwelling region, Rio de Janeiro, Brazil. Aquatic Botany, 52(4), 283-299.

Hamdan, N. A., Hassan, M. S. A., Noor, N. M., Hamid, S. A., & Bunnori, N. M. (2017). Dinoflagellates: Ecological approaches and spatial distributions in Malaysia waters. Journal of Sustainability Science and Management, 12(2), 1–26.

Henson, S. A., Cael, B. B., Allen, S. R., & Dutkiewicz, S. (2021). Future phytoplankton diversity in a changing climate. Nature communications, 12(1), 5372.

Huot, Y., Babin, M., Bruyant, F., Grob, C., Twardowski, M. S., & Claustre, H. (2007). Does chlorophyll a provide the best index of phytoplankton biomass for primary productivity studies?. Biogeosciences discussions, 4(2), 707-745.

IOCCG (2014). Phytoplankton Functional Types from Space. Sathyendranath, S. (ed.), Reports of the International Ocean-Colour Coordinating Group, No. 15, IOCCG, Dartmouth, Canada.

Islabão, C. A., Mendes, C. R. B., Detoni, A. M. S., & Odebrecht, C. (2017). Phytoplankton community structure in relation to hydrographic features along a coast-to-offshore transect on the SW Atlantic Continental Shelf. Continental Shelf Research, 151, 30-39.

Kim, J. H. (2009). Estimating classification error rate: Repeated cross-validation, repeated hold-out and bootstrap. Computational statistics & data analysis, 53(11), 3735-3745.

Konik, M., Pena, M. A., Hirawake, T., Hunt, B. P., Vishnu, P. S., Eisner, L. B., ... & Costa, M. (2024). Bioregionalization of the subarctic Pacific based on phytoplankton phenology and composition. Progress in Oceanography, 228, 103315.

Kramer, S. J., Siegel, D. A., Maritorena, S., & Catlett, D. (2022). Modeling surface ocean phytoplankton pigments from hyperspectral remote sensing reflectance on global scales. Remote Sensing of Environment, 270, 112879.

Kumar, A., & Mehta, M. (2024). Investigating the effect of relative spectral response on the estimation of atmospheric parameters: A case study of landsat 8 (OLI) and sentinel 2 (MSI). Journal of the Indian Society of Remote Sensing, 52(10), 2115-2122.

Lange, P. K., Werdell, P. J., Erickson, Z. K., Dall'Olmo, G., Brewin, R. J., Zubkov, M. V., ... & Cetinić, I. (2020). Radiometric approach for the detection of picophytoplankton assemblages across oceanic fronts. Optics Express, 28(18), 25682-25705.

Lee, Z., Ahn, Y. H., Mobley, C., & Arnone, R. (2010). Removal of surface-reflected light for the measurement of remote-sensing reflectance from an above-surface platform. Optics Express, 18(25), 26313-26324.

Lee, Z., Hu, C., Shang, S., Du, K., Lewis, M., Arnone, R., & Brewin, R. (2013). Penetration of UV‐visible solar radiation in the global oceans: Insights from ocean color remote sensing. Journal of Geophysical Research: Oceans, 118(9), 4241-4255.

Li, X., Yang, Y., Ishizaka, J., & Li, X. (2023). Global estimation of phytoplankton pigment concentrations from satellite data using a deep‐learning‐based model. Remote Sensing of Environment, 294, 113628

Lima, C. R., Mendes, C. R. B., Tavano, V. M., Detoni, A. M. S., & Secchi, E. R. (2019). Chemotaxonomy-based mapping of phytoplankton communities in the subtropical Southwestern Atlantic Ocean, with emphasis on the marine cyanobacterium Trichodesmium. Progress in Oceanography, 172, 77-88.

Lima, T. M. A. de, Giardino, C., Bresciani, M., Barbosa, C. C. F., Fabretto, A., Pellegrino, A., & Beglomini, F. N. (2023). Assessment of estimated phycocyanin and chlorophyll‐a concentration from PRISMA and OLCI in Brazilian inland waters: A comparison between semi‐analytical and machine learning algorithms. Remote Sensing, 15(5), 1299

Liu, H., Probert, I., Uitz, J., Claustre, H., Aris‐Brosou, S., Frada, M., Not, F., & de Vargas, C. (2009). Extreme diversity in noncalcifying haptophytes explains a major pigment paradox in open oceans. Proceedings of the National Academy of Sciences, 106(31), 12803–12808.

Mackey, M. D., Mackey, D. J., Higgins, H. W., & Wright, S. W. (1996). CHEMTAX-a program for estimating class abundances from chemical markers: application to HPLC measurements of phytoplankton. Marine Ecology Progress Series, 144, 265-283.

Marta-Almeida, M., Dalbosco, A., Franco, D., & Ruiz-Villarreal, M. (2021). Dynamics of river plumes in the South Brazilian Bight and South Brazil. Ocean Dynamics, 71(1), 59-80.

Mascarenhas, V., Keck, T., Mascarenhas, V., & Keck, T. (2018, August). Marine optics and ocean color remote sensing. In YOUMARES 8–Oceans Across Boundaries: Learning from each other: Proceedings of the 2017 conference for YOUng MARine RESearchers in Kiel, Germany (pp. 41-54). Cham: Springer International Publishing.

Mazzini, P. L. F., & Barth, J. A. (2013). A comparison of mechanisms generating vertical transport in the Brazilian coastal upwelling regions. Journal of Geophysical Research: Oceans, 118(11), 5977-5993.

McClain, C. R. (2009). A decade of satellite ocean color observations. Annual Review of Marine Science, 1(1), 19-42.

Meister, G., Knuble, J. J., Gliese, U., Bousquet, R., Chemerys, L. H., Choi, H., ... & Werdell, P. J. (2024). The ocean color instrument (OCI) on the plankton, aerosol, cloud, ocean ecosystem (PACE) mission: system design and prelaunch radiometric performance. IEEE Transactions on Geoscience and Remote Sensing, 62, 1-18.

Mendes, C.R., et al. 2007. HPLC determination of phytoplankton and microphytobenthos pigments: comparing resolution and sensitivity of a C18 and a C8

method. Limnol. Oceanogr. Methods 5, 363–370. https://doi.org/10.4319/lom.2007.5.363.

Mendes, C. R. B., Odebrecht, C., Tavano, V. M., & Abreu, P. C. (2017). Pigment-based chemotaxonomy of phytoplankton in the Patos Lagoon estuary (Brazil) and adjacent coast. Marine Biology Research, 13(1), 22-35.

Mnich, K., Polewko-Klim, A., Golińska, A. K., Lesiński, W., & Rudnicki, W. R. (2020, November). Super learning with repeated cross validation. In 2020 International Conference on Data Mining Workshops (ICDMW) (pp. 629-635). IEEE.

Mobley, C. D. (1999). Estimation of the remote-sensing reflectance from above-surface measurements. Applied optics, 38(36), 7442-7455.

Möller, O. O., Piola, A. R., Freitas, A. C., & Campos, E. J. (2008). The effects of river discharge and seasonal winds on the shelf off southeastern South America. Continental shelf research, 28(13), 1607-1624.

Morel, A., & Berthon, J. F. (1989). Surface pigments, algal biomass profiles, and potential production of the euphotic layer: Relationships reinvestigated in view of remote‐sensing applications. Limnology and oceanography, 34(8), 1545-1562.

Moser, G. A. O., Takanohashi, R. A., Braz, M. de C., Lima, D. T. de, Kirsten, F. V., Guerra, J. V., Fernandes, A. M., & Pollery, R. C. G. (2014). Phytoplankton spatial distribution on the Continental Shelf off Rio de Janeiro, from Paraíba do Sul River to Cabo Frio. Hydrobiologia, 728(1), 1–21.

Mouw, C. B., Hardman-Mountford, N. J., Alvain, S., Bracher, A., Brewin, R. J., Bricaud, A., ... & Uitz, J. (2017). A consumer's guide to satellite remote sensing of multiple phytoplankton groups in the global ocean. Frontiers in Marine Science, 4, 41.

Mueller, J. L., Morel, A., Frouin, R., Davis, C. O., Arnone, R., Carder, K. L., Lee, Z. P., Steward, R. G., Hooker, S. B., Mobley, C. D., McLean, S., Holbert, B., Miller, M., Pietras, C., Knobelspiesse, K. D., Fargion, G. S., Porter, J., & Voss, K. J. (2003). Ocean Optics Protocols for Satellite Ocean Color Sensor Validation, Revision 4, Volume III. NASA Goddard Space Flight Center.

Nair, A., Sathyendranath, S., Platt, T., Morales, J., Stuart, V., Forget, M. H., Devred, E., & Bouman, H. (2008). Remote sensing of phytoplankton functional types. Remote Sensing of Environment, 112(8), 3366-3375.

NASA Ocean Biology Processing Group. (2025a). PACE OCI Level-2 Regional Apparent Optical Properties Data, version 3.1 [Data set]. NASA Ocean Biology Distributed Active Archive Center. https://doi.org/10.5067/PACE/OCI/L2/OC_AOP/3.1

NASA Ocean Biology Processing Group. (2025b). PACE OCI Level-4 Regional Mapped Multi-Ordination ANAlysis (MOANA) Data, version 3.1 [Data set]. NASA Ocean Biology Distributed Active Archive Center. https://doi.org/10.5067/PACE/OCI/L4M/MOANA/3.1

Niroumand-Jadidi, M., Bovolo, F., & Bruzzone, L. (2020). Water quality retrieval from PRISMA hyperspectral images: First experience in a turbid lake and comparison with Sentinel-2. *Remote Sensing, 12*(23), 3984.

Pan, X., Mannino, A., Russ, M. E., Hooker, S. B., & Harding Jr, L. W. (2010). Remote sensing of phytoplankton pigment distribution in the United States northeast coast. Remote Sensing of Environment, 114(11), 2403-2416.

Pellegrino, A., Fabretto, A., Bresciani, M., et al. (2023). Assessing the accuracy of PRISMA standard reflectance products in globally distributed aquatic sites. *Remote Sensing, 15*(8), 2163.

Pezzi, L. P., de Souza, R. B., Acevedo, O., Wainer, I., Mata, M. M., Garcia, C. A., & de Camargo, R. (2009). Multiyear measurements of the oceanic and atmospheric boundary layers at the Brazil‐Malvinas confluence region. Journal of Geophysical Research: Atmospheres, 114(D19).

Piola, A. R., Campos, E. J., Möller Jr, O. O., Charo, M., & Martinez, C. (2000). Subtropical shelf front off eastern South America. Journal of Geophysical Research: Oceans, 105(C3), 6565-6578.

Piola, A. R., Möller Jr, O. O., Guerrero, R. A., & Campos, E. J. (2008a). Variability of the subtropical shelf front off eastern South America: Winter 2003 and summer 2004. Continental Shelf Research, 28(13), 1639-1648.

Piola, A. R., Romero, S. I., & Zajaczkovski, U. (2008b). Space–time variability of the Plata plume inferred from ocean color. Continental Shelf Research, 28(13), 1556-1567.

Pniewski, F. (2020). HPLC separation of cyanobacterial and algal photosynthetic pigments. Biologia, 75(2), 223-233.

Qu, F., Wang, Y., Yu, D., & Chen, N. (2024). High‐frequency monitoring reveals phytoplankton succession patterns and the role of cryptophyte in a subtropical river reservoir. Algal Research, 82, 103680.

Rodrigues, R. R., & Lorenzzetti, J. A. (2001). A numerical study of the effects of bottom topography and coastline geometry on the Southeast Brazilian coastal upwelling. Continental Shelf Research, 21(4), 371-394.

Rousseaux, C. S., & Gregg, W. W. (2015). Recent decadal trends in global phytoplankton composition. Global Biogeochemical Cycles, 29(10), 1674-1688.

Ruddick, K. G., De Cauwer, V., Park, Y. J., & Moore, G. (2006). Seaborne measurements of near infrared water‐leaving reflectance: The similarity spectrum for turbid waters. Limnology and Oceanography, 51(2), 1167-1179.

Ruddick, K. G., Voss, K., Boss, E., Castagna, A., Frouin, R., Gilerson, A., ... & Vendt, R. (2019). A review of protocols for fiducial reference measurements of water-leaving radiance for validation of satellite remote-sensing data over water. Remote Sensing, 11(19), 2198.

Rudorff, N. D. M., & Kampel, M. (2012). Orbital remote sensing of phytoplankton functional types: a new review. International Journal of Remote Sensing, 33(6), 1967–1990.

Sathyendranath, S., Watts, L., Devred, E., Platt, T., Caverhill, C., & Maass, H. (2004). Discrimination of diatoms from other phytoplankton using ocean-colour data. Marine Ecology Progress Series, 272, 59–68.

Schalles, J. F. (2006). Optical remote sensing techniques to estimate phytoplankton chlorophyll a concentrations in coastal waters with varying suspended matter and CDOM concentrations. In L. L. Richardson & E. F. LeDrew (Eds.), Remote sensing of aquatic coastal ecosystem processes: Science and management applications (pp. 27–79). Springer.

Smith, R. C., & Baker, K. S. (1984, September). The analysis of ocean optical data. In Ocean optics VII (Vol. 489, pp. 119-126). SPIE.

Smith, R. C., & Baker, K. S. (1986, August). Analysis of ocean optical data II. In Ocean Optics VIII (Vol. 637, pp. 95-107). SPIE.

Soares, I., & Möller Jr, O. (2001). Low-frequency currents and water mass spatial distribution on the southern Brazilian shelf. Continental Shelf Research, 21(16-17), 1785-1814.

Soja-Woźniak, M., Craig, S. E., Kratzer, S., Wojtasiewicz, B., Darecki, M., & Jones, C. T. (2017). A novel statistical approach for ocean colour estimation of inherent optical properties and cyanobacteria abundance in optically complex waters. Remote Sensing, 9(4), 343.

Soppa, M. A., Brell, M., Chabrillat, S., Alvarado, L. M., Gege, P., Plattner, S., ... & Bracher, A. (2024). Full mission evaluation of EnMAP water leaving reflectance products using three atmospheric correction processors. *Optics Express*, *32*(16), 28215-28230.

Steinmetz, F., Deschamps, P. Y., & Ramon, D. (2011). Atmospheric correction in presence of sun glint: application to MERIS. Opt. Express 19, 9783–9800. https://doi.org/10.1364/OE.19.009783.

Steinmetz, F., & Ramon, D. (2018). Sentinel-2 MSI and Sentinel-3 OLCI consistent ocean colour products using POLYMER, in: Proc. SPIE 10778, Remote Sensing of the Open and Coastal Ocean and Inland Waters. SPIE, p. 107780E. https://doi.org/10.1117/12.2500232.

Stoer, A. C., & Fennel, K. (2024). Carbon-centric dynamics of Earth's marine phytoplankton. Proceedings of the National Academy of Sciences, 121(45), e2405354121.

Sugiyama, K., & Takaichi, S. (2020). Carotenogenesis in cyanobacteria: CruA/CruP-type and CrtL-type lycopene cyclases. Journal of General and Applied Microbiology, 66(3), 123–130.

Taylor, B. B., Taylor, M. H., Dinter, T., & Bracher, A. (2013). Estimation of relative phycoerythrin concentrations from hyperspectral underwater radiance measurements—A statistical approach. Journal of Geophysical Research: Oceans, 118(6), 2948-2960.

Tréguer, P., Bowler, C., Moriceau, B., Dutkiewicz, S., Gehlen, M., Aumont, O., Bittner, L., Dugdale, R., Finkel, Z., Iudicone, D., Jahn, O., Guidi, L., Lasbleiz, M., Leblanc, K., Levy, M., & Pondaven, P. (2018). Influence of diatom diversity on the ocean biological carbon pump. Nature Geoscience, 11(1), 27–37.

Thomsen, H. A., Buck, K. R., & Chavez, F. P. (1994). Haptophytes as components of marine phytoplankton. In J. C. Green & B. S. C. Leadbeater (Eds.), The Haptophyte Algae (Vol. 51, pp. 187–208). Oxford University Press/Clarendon Press.

Vandermeulen, R., V. Lance, C, Otoshi, K. Riley, M. Tomlinson, and R. Trinh. 2025. Plankton, Aerosol, Cloud and ocean Ecosystem (PACE) satellite data for aquaculture and fisheries management. NOAA Tech. Memo. NMFS-F/SPO-255, 43 p.

Vanhellemont, Q., & Ruddick, K. (2016, May). Acolite for Sentinel-2: Aquatic applications of MSI imagery. In Proceedings of the 2016 ESA living planet symposium, Prague, Czech Republic (Vol. 9).

Vanhellemont, Q., & Ruddick, K. (2018). Atmospheric correction of metre-scale optical satellite data for inland and coastal water applications. Remote sensing of environment, 216, 586-597.

Verma, N., Lohrenz, S., Chakraborty, S., & Fichot, C. G. (2021). Underway hyperspectral bio-optical assessments of phytoplankton size classes in the river-influenced northern Gulf of Mexico. Remote Sensing, 13(17), 3346.

Vishnu, P. S., Xi, H., Belluz, J. D. B., Hussain, M. S., Bracher, A., & Costa, M. (2022). Seasonal dynamics of major phytoplankton functional types in the coastal waters of the west coast of Canada derived from OLCI Sentinel 3A. Frontiers in Marine Science, 9, 1018510.

Vishnu, P. S., Del Bel Belluz, J., Xi, H., Shah Hussain, M., Bracher, A., & Costa, M. (2025). Highly resolved surface phytoplankton community composition along the British Columbia Coast, derived from in situ hyperspectral radiometry. Journal of Geophysical Research: Biogeosciences, 130(10), e2025JG008956.

Werdell, P. J., Behrenfeld, M. J., Bontempi, P. S., Boss, E., Cairns, B., Davis, G. T., ... & Remer, L. A. (2019). The plankton, aerosol, cloud, ocean ecosystem mission: status, science, advances. Bulletin of the American Meteorological Society, 100(9), 1775-1794.

Werdell, P. J., Franz, B., Poulin, C., Allen, J., Cairns, B., Caplan, S., ... & Sirk, E. (2024, November). Life after launch: A snapshot of the first six months of NASA's Plankton, Aerosol, Cloud, Ocean Ecosystem (PACE) mission. In Sensors, Systems, and Next-Generation Satellites XXVIII (Vol. 13192, pp. 70-84). SPIE.

Westberry, T. K., Siegel, D. A., & Subramaniam, A. (2005). An improved bio-optical model for the remote sensing of Trichodesmium spp. blooms. Journal of Geophysical Research: Oceans, 110(C6).

Winder, M.; & Sommer, U. (2012). Phytoplankton response to a changing climate. Hydrobiologia, 698: 5-16.

Wright, S.W., et al. 2009. Composition and significance of picophytoplankton in Antarctic waters. Polar Biol. 32, 797–808. https://doi.org/10.1007/s00300-009-0582-9.

Xi, H., Hieronymi, M., Krasemann, H., & Röttgers, R. (2017). Phytoplankton group identification using simulated and in situ hyperspectral remote sensing reflectance. Frontiers in Marine Science, 4, 272.

Xi, H., Losa, S. N., Mangin, A., Soppa, M. A., Garnesson, P., Demaria, J., ... & Bracher, A. (2020). Global retrieval of phytoplankton functional types based on empirical orthogonal functions using CMEMS GlobColour merged products and further extension to OLCI data. Remote Sensing of Environment, 240, 111704.

Xi, H., Bretagnon, M., Losa, S. N., Brotas, V., Gomes, M., Peeken, I., ... & Bracher, A. (2023). Satellite monitoring of surface phytoplankton functional types in the Atlantic Ocean over 20 years (2002–2021). State of the Planet, 1, 1-13.

Yang, K., Wang, H., Dai, G., Hu, S., Zhang, Y., & Xu, J. (2011, October). Determining the repeat number of cross-validation. In 2011 4th International Conference on Biomedical Engineering and Informatics (BMEI) (Vol. 3, pp. 1706-1710). IEEE.

Zapata, M., Rodríguez, F., & Garrido, J. L. (2000). Separation of chlorophylls and carotenoids from marine phytoplankton: a new HPLC method using a reversed phase C8 column and pyridine-containing mobile phases. Marine Ecology Progress Series, 195, 29-45.

Zhang, X., He, S., Shabani, A., Zhai, P. W., & Du, K. (2017). Spectral sea surface reflectance of skylight. Optics Express, 25(4), A1-A13.

Zhang, Y., Lin, X., Shi, X., Lin, L., Luo, H., Li, L., & Lin, S. (2019). Metatranscriptomic signatures associated with phytoplankton regime shift from diatom dominance to a dinoflagellate bloom. Frontiers in Microbiology, 10, 590

Zhang, Y., Shen, F., Li, R., Li, M., Li, Z., & Sun, X. (2026). Global estimation of phytoplankton functional types using PACE OCI hyperspectral data and a novel deep ensemble learning approach. International Journal of Applied Earth Observation and Geoinformation, 148, 105225.

Zibordi, G., D'Alimonte, D., & Berthon, J. F. (2004). An evaluation of depth resolution requirements for optical profiling in coastal waters. Journal of Atmospheric and Oceanic Technology, 21(7), 1059-1073.

CAPÍTULO 3: CONCLUSÕES

A presente dissertação de mestrado teve como objetivo central propor modelos de estimativas de grupos funcionais de fitoplâncton (PFTs) a partir de composição pigmentar e da reflectância hiperespectral de superfície, em uma região costeira, visando sua aplicação desses em dados satelitais. A área de estudo englobou águas costeiras do Oceano Atlântico Sudoeste (SWAO), uma região opticamente complexa (águas do Caso 2). Para tal modelagem, foi empregada uma abordagem baseada em de Funções Ortogonais Empíricas (EOF), adaptada de Bracher et al. (2015). Os resultados demonstraram que o modelo proposto foi bem-sucedido ($R_cv \geq 0,7$ e p-valor $< 0,0001$) na estimativa da TChla e de cinco grupos funcionais do fitoplâncton (diatomáceas, criptófitas, dinoflagelados, haptófitas e prasinófitas), enquanto obteve desempenho moderado para *Prochlorococcus* ($R_cv \geq 0,5$) e insatisfatório para *Synechococcus* ($R_cv < 0,5$). Dessa forma, os objetivos originais da pesquisa foram atendidos de maneira ampla, com a ressalva das limitações inerentes à estimativa de cianobactérias em ambientes costeiros.

Do ponto de vista teórico, a presente dissertação traz avanços ao demonstrar que métodos empíricos baseados em EOF, tradicionalmente aplicados em águas oceânicas (Caso 1), podem ser adaptados com sucesso para regiões costeiras opticamente complexas, onde o sinal de reflectância é dominado não apenas pela água pura e fitoplâncton, mas também por matéria orgânica dissolvida colorida (CDOM), material particulado em suspensão (TSM) e partículas não-algais (NAP). Na análise dos modos da EOF encontrou-se que a maior parte da variabilidade estava contida nos primeiros quatro modos de variabilidade, de forma que foi possível caracterizar os principais componentes opticamente ativos, contribuindo para a compreensão dos padrões ópticos da área de estudo. De forma prática, foi possível utilizar a compreensão desses padrões ópticos para propor modelos para estimar a concentração da Clorofila-*a* Total (TChla) e a da Chla de PFT elencado.

Ao se realizar um primeiro exemplo de uso dos modelos propostos em uma imagem, do sensor OCI/PACE, pode-se observar padrões de distribuição espacial dos PFTs, marcando um gradiente costa-oceano, com dominância de diatomáceas em regiões

costeiras eutróficas e de cianobactérias em águas oligotróficas oceânicas. Os achados são ecologicamente consistentes com o conhecimento oceanográfico consolidado para o Atlântico Sudoeste, conforme o conhecimento oceanográfico estabelecido para a região. Isso nos fornece uma primeira evidência de que os modelos propostos podem ser aplicados com confiabilidade em produtos oriundos de sensoriamento remoto, requerendo ainda uma posterior validação extensa com dados independentes.

A capacidade de estimar a composição funcional do fitoplâncton em alta resolução espaço-temporal a partir de dados hiperespectrais orbitais têm aplicações diretas na gestão de ecossistemas costeiros, no monitoramento de florações de algas nocivas (FANs), na aquicultura, na modelagem pesqueira e na conservação marinha. Em um contexto mais amplo, a capacidade de discriminar grupos funcionais a partir do espaço permite que pesquisadores e agências governamentais aprimorem a parametrização de ciclos biogeoquímicos em modelos climáticos, reduzindo incertezas associadas ao papel do oceano no sequestro de carbono. A inclusão de informações sobre a composição da comunidade fitoplanctônica, não apenas sua biomassa total, torna as projeções sobre o futuro do ciclo do carbono mais realistas e robustas.

Apesar dos avanços, também foram identificadas limitações importantes que devem ser solucionadas em pesquisas futuras. O desempenho inferior para cianobactérias, especialmente do *Synechococcus*, foi atribuído à reduzida faixa de variação das concentrações desse grupo observadas no conjunto de treinamento, assim como a limitação do método em relação ao pigmento marcador zeaxantina e à ausência da temperatura da superfície do mar (SST) como variável preditora do modelo. Recomenda-se, portanto, a incorporação de novas amostras de treinamento na modelagem, prioritariamente em locais onde as cianobactérias apresentem um sinal dominante ou concentrações mais elevadas, de modo a expandir a faixa dinâmica do modelo e reduzir artefatos de subestimativa e de saturação. Sugere-se, ainda, testar a inclusão da SST como covariável em futuras iterações do modelo.